UNIVERSITY OF HELSINKI REPORT SERIES IN PHYSICS

HU-P-D201

Progress in Elastic Recoil Detection Analysis

Kenichiro Mizohata

Division of Materials Physics
Department of Physics
Faculty of Science
University of Helsinki
Helsinki, Finland

ACADEMIC DISSERTATION

To be presented, with the permission of the Faculty of Science of the University of Helsinki, for public criticism in the Auditorium (A129) of Chemicum, on December 14th, 2012 at 12 o'clock noon.

HELSINKI 2012

ISBN 978-952-10-8088-3 (printed version)
ISSN 0356-0961
Helsinki 2012
Yliopistopaino

ISBN 978-952-10-8089-0 (PDF version)
http://ethesis.helsinki.fi/
Helsinki 2012
Helsingin yliopiston verkkojulkaisut

Kenichiro Mizohata: **Progress in Elastic Recoil Detection Analysis**, University of Helsinki, 2012, 53 p.+appendices, University of Helsinki Report Series in Physics, HU-P-D201 ISSN 0356-0961, ISBN 978-952-10-8088-3 (printed version), ISBN 978-952-10-8089-0 (PDF version)

Classification (PACS): 07.57.-c, 81.70.-q, 81.07.Bc, 81.05.Lg 81.05.Je
Keywords: ion beam analysis, elastic recoil detection, time of flight detector, gas ionisation detector, stopping force, surface analysis, depth resolution

ABSTRACT

Elastic recoil detection analysis (ERDA) with heavy ion beams has evolved into a universal ion beam analysis (IBA) method for simultaneous analysis of almost all elements, with an essentially constant detection sensitivity. The method is based on the detection and identification of recoiling atoms that have been elastically scattered from a sample by an incident heavy ion beam.

The principal characteristics of heavy-ion ERDA are outlined and illustrated using examples of data obtained with time of flight (TOF) and $\Delta E - E$ detector systems. The potential and limitations of the quantitative analysis were explored. For this purpose, a number of thin layer samples were measured using different projectiles and energies.

Desorption of the surface materials during ERDA measurements was determined as a function of the probing ion fluence. As the differential cross-sections for scattering were enhanced for heavy projectiles, the beam dose to which the sample was exposed to during measurements was reduced by using heavy ion beams. However the higher cross-sections caused an increase of the desorption.

An essential part of this study was dedicated to study those topics that limit the accuracy of the analysis in heavy ion TOF-ERDA, namely: uncertain stopping forces, quantification accuracy, irradiation induced damage, depth resolution, and the role of multiple and plural scattering.

Possible approaches to improve the sample characterisation efficiency and accuracy were studied by using a gas ionisation detector. This study concentrates on the noise reduction, detection characterisation, and analysis procedures. The focus was upon the effect of the large solid angle and position sensitivity on the irradiation induced damage, depth resolution, mass resolution, and elemental sensitivity.

The reliability of the concentration distributions obtained with heavy ion ERDA was strongly affected by the surface structure, surface roughness and multiple scattering. These effects were studied by comparing Monte Carlo simulations with the experimental results.

The analysis procedure was developed to enable the characterisation of novel materials such as atomic layer deposited thin films and nanoparticles. Data handling and storage was improved to facilitate and speed up the analysis procedures.

Contents

1 Introduction

Materials research corresponds to progressive fields of research and technology. The characterisation of the underlying structures of the materials are far beyond the analytical limits of most conventional methods due to continuous miniaturisation of these structures. However ion beam analysis (IBA) methods provide ways to study such structures as they use probes of similar or much smaller dimensions than the target samples. IBA methods represent one of the applied branches of the contemporary physics that has increasing importance in developing modern materials. Although some of the methods have been known for many years, the constant progress in accelerator and detector technologies, and the continuous expansion of the required databases permit an extended application of IBA methods.

Charged particle IBA methods combined with neutron activation analysis in addition to the many different variations of electron spectroscopy can be used for analysis of thin films and surface layers of materials that are difficult to investigate by conventional non-nuclear methods. IBA methods provide information about the elemental composition over the whole range of the periodic system regardless of whether the elements of interest are in bulk or trace quantities. They also give information about the elemental depth distribution and the surface properties of the studied materials.

The IBA methods are utilised to study samples in materials research, industry, micro- and nanotechnology, electronics, optics and laser technology, chemical, biological, and environmental research in general. The advantage of using the IBA methods is that they can probe samples non-destructively, i.e. they leave the sample undamaged or damage created is not visible to the eye.

IBA utilises ion beams of various elements with kinetic energies that range from hundreds of kiloelectronvolts up to hundreds of megaelectronvolts, and beam currents mostly within tens of nanoamperes range. The data on the studied samples are provided via the measurements of the energy spectra of scattered ions, recoiled atoms, and the secondary radiation induced by ion bombardment.

IBA methods is based on the investigation of the elastic collisions between projectiles and the target atoms of the sample or on detection of products of inelastic processes such as electronic excitation and nuclear reactions. The well-known Rutherford Backscattering Spectrometry (RBS) is based on the detection of light projectile ions that elastically scatter backwards from heavier

sample atoms. A typical setup for RBS utilises either beams of protons or He ions, with kinetic energies of several MeV. Energy spectra of the scattered projectiles provide information about the sample. The kinematics of the elastic collision process are such that RBS is capable to detect all the elements that are heavier than the projectile ion with detection limits down to 10^{-12} at/cm^2 [1]. It also allows depth profiling of the target surface layers of tens of micrometers thick with a depth resolution of nanometers.

Elastic recoil detection analysis (ERDA) is a complementary analytical method to RBS. It is based on a principle that is the inverse of RBS. In the first successful application [2] recoil atoms of heavy projectiles were produced using incident 25-40 MeV ^{35}Cl ions. In ERDA heavy projectiles at energies up to several hundreds of MeV collide with sample atoms and knock them out of the sample in the forward direction, where a particle detector locates and measures the energy of the recoiled atoms. The acquisition and evaluation of energy spectra of the recoiled atoms is complicated by the presence of elastically scattered primary ions. However, several ERDA arrangements have been constructed to overcome this difficulty [3]. The scattered primary ions may simply be absorbed by a thin foil placed in front of the energy detector. Another approach is the simultaneous detection of both the scattered primary ions and recoiled atoms, or by using of a special detector to differentiate the primary and the recoiled atoms. The time of flight ERDA (TOF-ERDA) method [4, 5], has become a very useful IBA method. Generally, the ERDA method can be used to detect all elements that are lighter than the projectile ion and with special detectors also elements that are heavier than the projectile. It also allows depth profiling layers of up to several micrometers with nanometer depth resolutions. The detection limits are comparable to those of RBS [1].

The availability of reliable experimental stopping force data is of critical importance for many ion beam applications. From the point of view of fundamental physics, the ion-matter interaction models based on first-principles are still far from the accuracy and generality desired for practical applications. Therefore, experimental data are required to evaluate these models and to introduce possible improvements that would lead to a better understanding of the dynamics of charged particles in matter. On the other hand, semi-empirical models may offer reasonable precision and to a certain extent, may be even able to predict the stopping forces for ion-target combinations that have not been explored experimentally. However, these semi-empirical models need large amounts of experimental data on stopping since their accuracy depends on how this type of available information is fitted.

From the IBA perspective, the need for accurate data on stopping forces for ions is clear. ERDA makes use of the energy lost by ions in a sample to gain information about the compositional depth profiles. Therefore, the accuracy and precision of the depth profiles are directly associated with the corresponding accuracy and precision of the available stopping force values for every ion-material combination measured in an experiment. The energy loss of charged particles in matter is also related to the damage created in the samples by the incident ions and recoiling atoms.

2 Purpose and structure of this study

The main purpose of this study was to improve heavy ion elastic recoil detection analysis (HI-ERDA) to meet the analysis demands of the Finnish Centre of Excellence in Atomic Layer Deposition. The atomic layer deposited samples to be studied consist of thin films, microstructures, nanostructures, in addition to materials for microelectronics and energy technologies.

This thesis consists of a summary and three published articles and a fourth article that has been submitted for publication in international peer-reviewed journals. The publications are listed below, included after the summary, and referred to in the text by Roman numerals. Principles of the elastic recoil detection method are summarised in section 3, the progress and results in the analysis and measurements are described in section 4. Conclusions and outlook are presented in section 5.

2.1 Original publications contributing the thesis

The following articles are included in this thesis.

Publication I: Stopping forces of polyimide, vyns, formvar, and polysulfone for Cl, Br, and I ions,
K. Mizohata, J. Keinonen, J. Räisänen, *Nuclear Instruments and Methods in Physics Research B* **280**, (2012), 74–78.

Publication II: Stopping cross sections of atomic layer deposited Al_2O_3 and Ta_2O_5 and of Si_3N_4 for ^{12}C, ^{16}O, ^{35}Cl, ^{79}Br and ^{127}I ions,
K. Mizohata, J. Keinonen, J. Räisänen, E. Härkönen, J. Palmans, M. Ritala, *Nuclear Instruments and Methods in Physics Research B*, Submitted for publication.

Publication III: A Pyrazolate-based metalorganic tantalum precursor that exhibits high thermal stability and its use in the atomic layer deposition of Ta(2)O(5),
C. L. Dezelah IV, M. K. Wiedmann, K. Mizohata, R. J. Baird, L. Niinistö, C. H. Winter, *J. Am. Chem. Soc.* **129**, (2007), 12370-12371.

Publication IV: Optical and structural properties of silicon-rich silicon oxide films: Comparison of ion implantation and molecular beam deposition methods,

T. Nikitin, K. Aitola, S. Novikov, M. Räsänen, R. Velagapudi, J. Sainio, J. Lahtinen, K. Mizohata, T. Ahlgren, L. Khriachtchev, *physica status solidi a*, **208**, (2011), 2176–2181.

2.2 Author's contributions

The accuracy of the IBA techniques to characterise materials is limited by several issues, such as the accuracy of the stopping forces, multiple scattering, and surface roughness. Inaccuracies of the stopping forces affect the accuracy of the material composition analysis and also that of the determination of film thicknesses. In publications I and II, the time of flight ERDA setup was used to determine stopping forces of several compound materials for ions used routinely in HI-ERDA measurements. The author designed and set up the measurements, improved the computer codes used, and analysed the data. The author was the responsible author and had a major contribution in writing of papers I and II.

In publication III, ERDA was used for the analysis of atomic layer deposited (ALD) thin films.

Publication IV is a study in which ERDA was used for the analysis of silicon-rich silicon oxide films.

The ERDA method also has applications in fields beyond thin films. Thus experiments and analysis of samples with nanoparticles and 3D structures were made. The developed ERDA technique was utilised in publications III and IV for which the author made the ERDA measurements, analysis and simulations. In publication IV implanted excess silicon in silica forming silicon nanocrystals was analysed. The progress in the ERDA obtained over the course of this stydy has been applied to analyse samples with gold nanoparticles [6] and solar thermal absorber coatings with copper particles on the sample surface [7] and in several other publications [8–12].

The feasibilities of two detection methods, namely the time of flight (TOF) and the gas ionisation detector for use in heavy ion ERDA with a 5 MV tandem accelerator were studied and compared. The design and construction of the gas ionisation detector were described in the studies included in this thesis. The author carried out all measurements, simulations and analysis of the results of the detector feasibility studies.

The progress in the development of the analysis procedure, data handling, analysis software and for the simulations carried out in this study are described in chapter 4.

3 Principles of elastic recoil detection analysis

ERDA is a technique suitable for the characterisation of thin films, determining sample composition and the elemental depth profiles. The kinematics and the cross-sections of the collisions between ions and sample atoms, in addition to the energy loss of ions and recoil atoms in the matter, regulate the quantification and the extraction of depth profiles.

HI-ERDA is usually equipped with an element or mass sensitive detector, in order to identify the recoiled sample atoms and scattered incident ions. The significant improvement in HI-ERDA over that of traditional ERDA is that quantitative depth profiling of all sample atoms can be provided by only one measurement [13–21]. A wide variety of ion beams and different energies are used in different laboratories, depending on the accelerator facility and the detection system. Typical ions used are ^{35}Cl, ^{63}Cu, ^{79}Br,^{127}I, and ^{197}Au, accelerated at energies up to few hundreds of MeV. The most common detection systems are magnetic spectrographs, TOF telescopes and gas ionisation detectors. For example, high energetic heavy ions such as 200 MeV ^{197}Au beams can be used in combination with a gas ionisation detector. Alternatively, medium heavy ions with energies tens of MeV such as 35 MeV ^{35}Cl beams are typically used with a TOF telescope.

The energy of a recoiled sample atom is measured and a knowledge of the stopping forces, scattering cross sections and scattering kinematics is used to determine the concentration distributions of the elements in the sample. Kinematics of the atom collisions and the scattering cross sections are well known at the energies (0.1 MeV/u–2 MeV/u) used in typical ERDA measurements. The stopping forces used in the analysis can differ by as much as 20% from the actual measured stopping forces. The lack of experimental data for heavy ions is a typical problem.

The performance of a technique depends on the setup and the experimental conditions. The achievable surface depth resolution is of the order of nanometers. The sensitivity is better than 0.1 atomic percent for all elements. In HI-ERDA, some factors, such as multiple scattering and ion beam induced damage, must be taken into consideration. These two phenomena can affect the interpretation of the data and the accuracy of the quantification. In addition, the glancing angles of in-going and out-coming particles highlight the importance of the surface topography related effects in the interpretation of the results. A reliable elemental characterisation of the surface layers can be obtained, when the surface topography information into the ion beam analysis is included.

The advantage of using the ERDA approach is the relatively simple analysis procedure compared to other procedures. Elemental quantification can be expressed as absolute or relative. The absolute concentration indicates the total number of atoms of a certain element present in a sample area and is normally expressed in 10^{15} at./cm^2. It can be derived either from the total beam fluence or by normalising the signal of the substrate intensity in the energy spectrum. The former procedure can be used when the detector solid angle and detection efficiency value are precisely known. This method requires the accurate measurement of the beam dose to obtain the total number of incident ions during the measurement.

The relative concentrations of constituent elements of a sample can be directly derived from the respective number of detected events for different elements, weighted according to its corresponding scattering cross-section. The complete sample structure and elemental profiling are normally obtained by the use of simulation programs. For any given experimental setup and conditions, these programs generate a scattering energy profile that is then compared to the experimental profile under study. The sample structure and composition are subsequently adjusted until the simulated spectrum corresponds to the experimental spectrum.

In ERDA, all elements present in a sample can be separately detected, and their respective depth profiles can be simultaneously generated from energy spectra using an iterative procedure. First, the sample is assumed to be homogeneous with the mean concentrations and the depths of origin are calculated for each detected recoiled constituent ion using the parameters of the measurement setup. The calculated recoil depths are then used to indicate a putative sample composition and to calculate stopping forces for this composition. The depth calculation is repeated and a new or modified composition is predicted. Typically, after four or five iterations, the calculated depth profiles are have stabilised.

3.1 Concentration analysis

3.1.1 Kinematics

When a beam of ions strikes a solid target, energy is transferred from the incident projectile ion to the target atom. This process is described by kinematic equations of elastic collisions. In a classical two-body elastic collision (fig. 1), the final energy of both particles can be calculated exactly. In

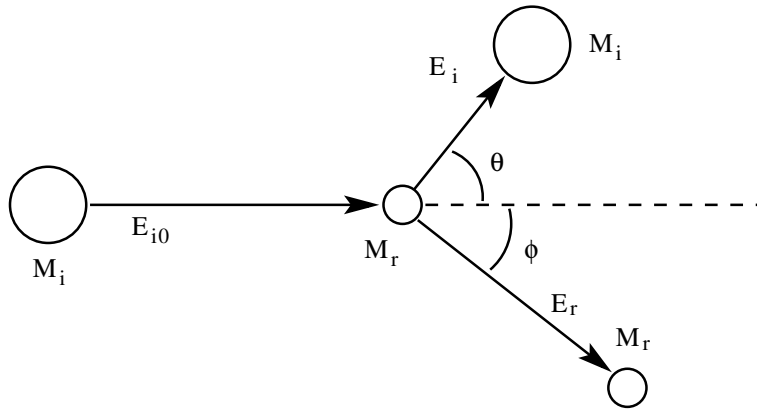

Figure 1: Schematic picture of a elastic scattering. The subscripts i and r denote incident ion and recoiling atom, respectively

the laboratory co-ordinates, the final energy of a recoiling atom calculated from the energy and momentum conservation laws is given by the following:

$$E_r = \left(\frac{4M_i M_r \cos^2 \phi}{(M_i + M_r)^2} \right) E_{i_0} \equiv \Lambda E_{i_0}, \tag{1}$$

where ϕ is the recoil angle and Λ is the kinematic factor for the recoil. Similarly the energy of scattered projectile is

$$E_i = E_{i_0} - E_r = \left(\frac{\sqrt{M_r^2 + M_i^2 \sin^2 \theta} \pm M_i \cos \theta}{M_i + M_r} \right)^2 E_{i_0} \equiv K E_{i_0}, \tag{2}$$

where θ is the scattering angle and K the kinematic factor for the scattered projectile. The mass ratio dependence of the kinematic factors for recoils and scattered projectiles for different detection angles are shown in fig. 2. The angular dependence of the kinematic factors in the case where the projectile is lighter or heavier than the sample atom, is illustrated in fig. 3.

At energies used in this study the only force present in a collision is the Coulomb repulsion between two nuclei. The Coulomb potential is in given by the term:

$$V(r) = \frac{1}{4\pi\varepsilon_0} \frac{Z_i Z_r e^2}{r}, \tag{3}$$

where Z_i and Z_r are the respective nuclear charges of the ion and target atom, and r is the distance between them.

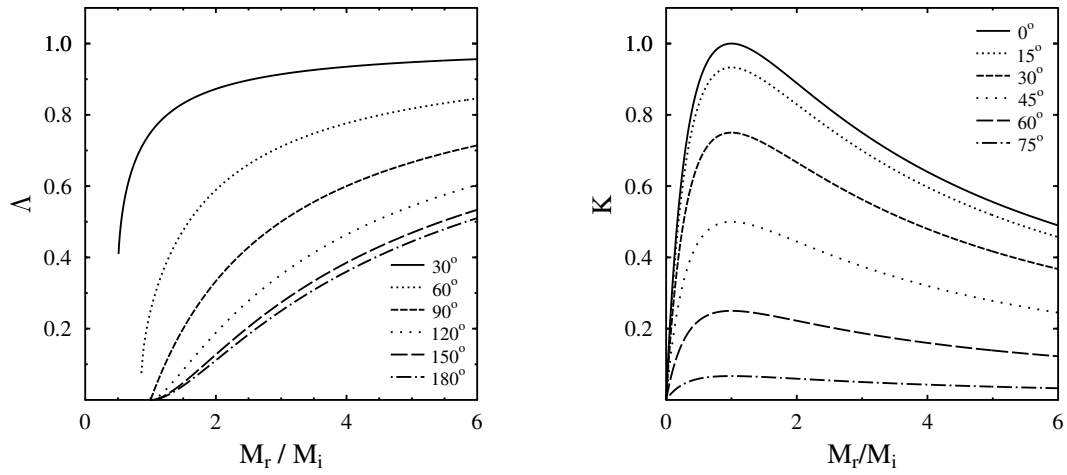

Figure 2: Kinematic factors for the scattered ions (K_s) and for the recoil atoms (K_r) as a function of the mass ratio M_2/M_1.

The probability of the elastic scattering is described by the scattering cross section. The differential scattering cross section gives the probability that the projectile ion scatters or target atom recoils into a solid angle. The differential scattering cross-section [1] derived from the respective Coulomb interaction is given by

$$\frac{d\sigma_S}{d\Omega} = \left(\frac{e^2}{8\pi\varepsilon_0}\frac{Z_1 Z_2}{E_0}\right)^2 \frac{\left(\sqrt{M_2^2 - M_1^2\sin^2\theta} \pm M_2\cos\theta\right)^2}{M_2\sin^4\theta\sqrt{M_2^2 - M_1^2\sin^2\theta}}. \tag{4}$$

The differential elastic cross-section for the recoil is:

$$\frac{d\sigma_R}{d\Omega} = \left(\frac{e^2}{8\pi\varepsilon_0}\frac{Z_1 Z_2}{E_0}\right)^2 \frac{(1+M_1/M_2)^2}{\cos^3\phi}. \tag{5}$$

Angular dependence of the scattering and recoil cross-sections are inverse as shown in fig. 3.

The scattering cross-section defines the elemental sensitivity of ERDA. The recoil yield is the measured signal that carries the required information. Ignoring sample properties such as composition and surface properties and dispersion phenomena such as straggling and multiple scattering, the

yield is given in the following expression

$$Y = qn_0 S\Omega_{det} * \frac{d\sigma_R}{d\Omega} \frac{x}{\sin\alpha}, \tag{6}$$

where q denotes projectile fluence, n_0 target atomic density, S the cross sectional area of the beam spot on the sample surface. Ω_{det} is the detector solid angle and the last term $\frac{d\sigma_R}{d\Omega}\frac{x}{\sin\alpha}$ expresses the length of the projectile path in an analyzed surface layer with thickness x, and α denoting the projectile incident angle.

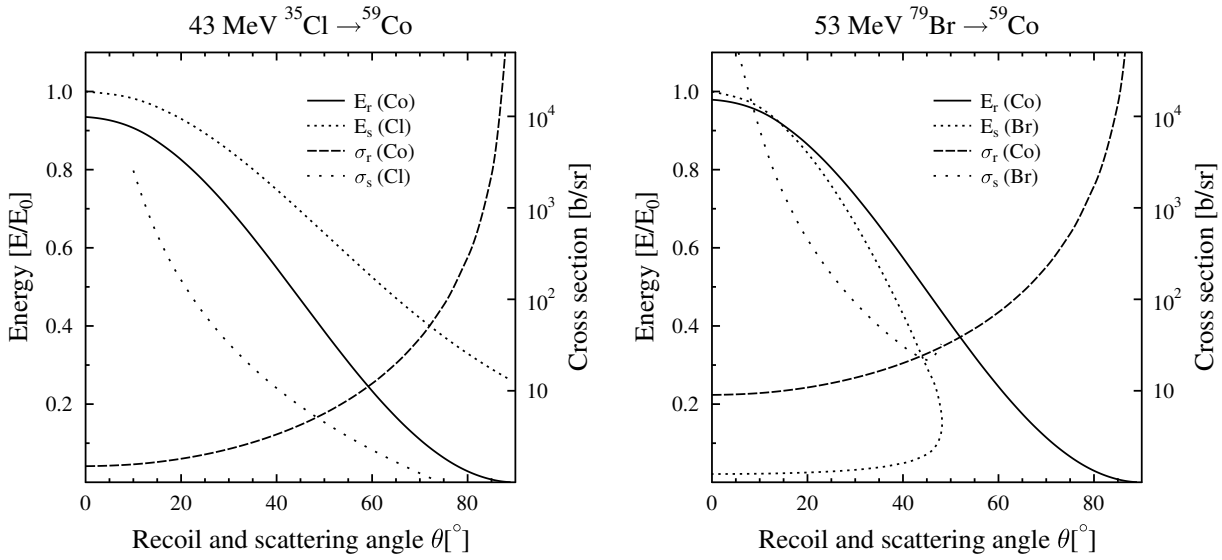

Figure 3: Elastic scattering energies and cross-sections of recoil atoms and scattered projectiles as a function of the scattering angle, when the primary ion is lighter (a) or heavier (b) than the target atom.

The scattering cross-sections, equations 4 and 5 can not be applied when the interaction potential deviates from the pure Coulomb potential of equation 3. Deviations from the Rutherford scattering occur both at high and low energies for all projectile-target pairs. The projectile energy E_T, above which the cross section value deviates from the Rutherford value, depends linearly both on Z_1 and Z_2 [22]. Above E_T nuclear reactions and inelastic scattering may take place.

3.2 Depth analyses

3.2.1 Ion energy loss

The concentration distributions obtained in ERDA are defined by the energy losses of the impinging ions and the recoiling atoms in a sample material. The energy loss in inelastic collisions with electrons of the atoms of the slowing down material, is called the electronic energy loss. The energy loss due to elastic collisions between a moving ion or recoil atom and a sample atom is called the nuclear energy loss. The total energy loss is described by the stopping force thus:

$$S(E) = -\frac{dE}{dx} = -\left[\left(\frac{dE}{dx}\right)_n + \left(\frac{dE}{dx}\right)_e\right], \tag{7}$$

where indexes n and e refer to nuclear and electronic stopping force, respectively. The total energy loss for an ion and recoil atom traversing a distance Δx in the material is then given by the following:

$$\Delta E = \int_0^{\Delta x} S dx. \tag{8}$$

The concept of the two independent components of the stopping forces is an approximation since there is a strong correlation between the location of electrons and the nuclei of target atoms. However, as in most practical cases there are other sources of uncertainties in the stopping models which greatly exceed the uncertainties introduced by the separate treatment of electronic and nuclear stopping forces.

The penetrating ions produce damage in the slowing down materials by breaking atomic bonds and causing atoms to recoil from their lattice sites. The slowing down of these recoiling atoms produce most of the damage in the sample material.

As opposed to the electronic energy loss, nuclear scattering causes large directional changes in the ion trajectories. These changes cause the energy and angular straggling of an ion traversing in a material to occur. Such straggling effects are important in ERDA.

Ion stopping of a sample made of a mixture of elements or of compounds can be estimated assuming that the interaction processes between the projectiles and target atoms are independent. This is called Bragg's rule [23] for the stopping cross-section. For a compound or mixture M_aN_b where

M and N are two different elements and a and b are their stoichiometric coefficients that have been normalised to unity, the total stopping cross-section ε_{MN} is given by

$$\varepsilon_{MN} = a\varepsilon_M + b\varepsilon_N, \tag{9}$$

where ε_M and ε_N are the stopping cross-sections of pure elements M and N.

This rule is reasonably accurate, and the measured stopping of ions in compounds usually deviates by less than 20% from those predicted by Bragg's rule. However in modern industrial applications and research, more accurate knowledge of stopping forces and ranges of ions in materials are needed. The accuracy of Bragg's rule is limited because the energy loss to the electrons in any material depends on their respective specific orbital and excitation structure energies, thus differences between elemental materials and the same atoms in compounds will cause Bragg's rule to become inaccurate. Furthermore, any bonding changes may also alter the charge state of the ion, thus changing the strength of its interaction with the target medium. The Core and Bond (CAB) approach suggests that stopping forces in compounds can be predicted by using the superposition of stopping by atomic "cores" and then adding the stopping due to the bonding electrons [24–27]. The core stopping would simply follow Bragg's rule for the atoms of the compound. The chemical bonds of the compound would then contain the necessary stopping correction.

3.2.2 Straggling

When ions penetrate a target medium, they undergo a large number of collisions with electrons and nuclei of atoms. As a consequence of the statistical nature of these processes, the numbers of collisions vary for each ion. Originally mono-energetic and mono-directional beam projectiles lose and change their direction of motion in varying ways. The resulting energy and directional distributions is related to with the distance travelled within the target. The energy spread caused by the interactions with the electrons is better known as energy straggling.

Collisions of heavy ions with electrons mainly entail energy straggling whereas the direction of motion remains almost the same. In contrast, subsequent collisions with target nuclei, so-called multiple scattering, lead to both energy and directional straggling. The resulting distributions are roughly Gaussian. Assuming a large number of collisions and a small relative energy loss, Bohr's

model also predicts a Gaussian energy distribution. The variance Ω_B^2 of the energy distribution is given by the expression:

$$\Omega_B^2 = 4\pi(Z_1 e^2)^2 N Z_2 \Delta x, \tag{10}$$

where $Z_2 N \Delta x$ is the number of electrons per unit area over the path length Δx. Corrections to Bohr's model take in to account charge state fluctuations and expand the model to a wider energy range [28–30].

In ERDA, multiple scattering, generates an angular distribution of the recoiling atoms around the its original recoil direction. Additionally, atoms may undergo more than one scattering event with a large scattering angle before they are scattered towards the detector, which is known as plural scattering. Although these events are scarce, they can play an important role in the analysis.

Multiple scattering has been reviewed by Szilagy et al. [31] and Amsel et al. [32]. Plural scattering can be treated fully with Monte Carlo simulations [33, 34]. A comparison of analytic calculations and Monte Carlo simulation for light and heavy incident ions has recently been published [35, 36].

The original precise measurement geometry is no longer valid due to the angular spread of the recoiling atoms. Multiple and plural scattering, result in a spread of both the path lengths and the scattering angle around the detection angle. The former generates a spreading in energy and also in the energy straggling of ions after penetration at a given depth. In contrast, the spread in the scattering angle has consequences for both the kinematics and the cross-sections associated with the total scattering process.

4 Progress in elastic recoil detection measurements

Requirements in the analyses of thin films and surface layers of materials are very demanding. Characteristics such as film composition, elemental profiling and surface structure are always significant and therefore need to be accurately measured. A list of requirement to do this consists of the following prerequisites:

1. Detection capability of all elements present in the sample, from Hydrogen to heavy elements.
2. Separation of signals originating from constituent elements of the sample. Capacity to distinguish and identify two different elements independently of the physical and chemical composition of the sample.
3. Depth resolution at the nanometer scale. A high depth resolution is necessary for films only a few nanometers thick in order to extract information on the surface and interface quality and on the elemental profiling inside the film.
4. Capability of probing the film throughout its whole thickness.
5. Detection accuracy in absolute elemental quantification, an areal density determination, and in depth profiling. High detection sensitivity.
6. Information on the sample crystallinity.

The aim of this study was to improve ERDA techniques and overcome several substantial limitations of ERDA and to study their applicability to the characterisation of thin films.

4.1 Detection of recoiled atoms

The ERDA techniques using equipment fitted with special detectors allow the separation of different recoil species. Different elements can be separated by either their nuclear charge or by their mass. TOF and gas ionization detectors such as the Bragg detector and various types of ΔE–E detectors have been developed to achieve this separation.

Typical ion beams used in this study were ^{35}Cl, ^{79}Br and ^{127}I beams, accelerated by a 5 MV tandem accelerator in the laboratory. The detector angle was determined to be 40.0 $\pm$ 0.1° by comparing the yields of scattered and recoiled ions from thin sample films. Typically the measurements were taken geometrically whereby both the incident and exit angles where equal to 20° to the sample surface.

4.1.1 Time of Flight telescope

The TOF-ERDA setup of the University of Helsinki consists of two timing gates and of an ion-implanted energy detector. A detailed description of the measurement system is given in Refs. [17, 37] and in fig. 4. The timing gates are fitted with a thin diamond like carbon (DLC) film, which have thicknesses that ranged from 4.7 and 9.0 μg/cm^2 in the first and second timing gates, respectively. Secondary electrons are emitted as the ions pass through the films. The electrons are accelerated and guided by an electrostatic field to micro-channel-plates (MCP) where they are multiplied. The electrons are collected at an anode, and the anode signal is directed to a constant fraction discriminator. The signals from the timing gates were then directed to a time-to-digital converter. An ion-implanted detector of the Ortec Ultra series was used in this thesis as the energy detector.

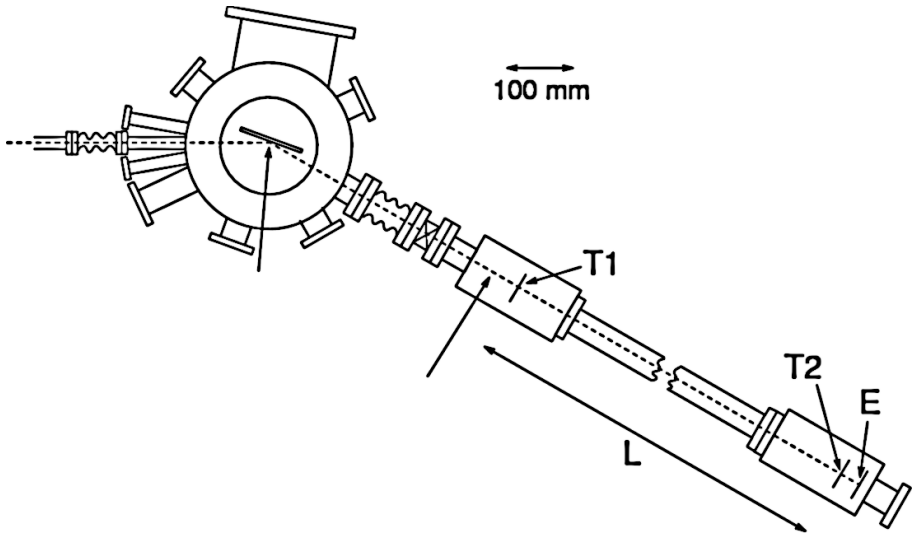

Figure 4: Schema of the ToF telescope detector. The scattering angle is 40°. The distance L between the timing gates T1 and T2 is 684 mm.

TOF spectrometers have a detection efficiency that is energy and ion dependent and is typically less than 100% for light ions [38–40]. For a setup with two timing gates, the total detection efficiency is given by the expression

$$\varepsilon = \varepsilon_{T1} \cdot \varepsilon_{T2} \cdot T_C, \tag{11}$$

where ε_{T1} and ε_{T2} are the efficiencies of the timing gates and the last term is the contribution of the scattering in the first carbon foil.

The detection efficiency of the timing gates is limited by the secondary electron yield of the foil. The mean number of ejected secondary electrons is directly proportional to the electronic stopping force [41], in the following expression:

$$Y = \Lambda \frac{dE}{dx} \tag{12}$$

with the coefficient Λ depending on the atomic number and energy of the incident ion. Values of Λ for secondary electron yields emitted by a carbon foil, both for forward Λ_F and backward Λ_B directions decrease with increasing atomic mass [41, 42]. The electron yield is lower in the backward direction, with a ratio Λ_F/Λ_B that ranges from ~ 1.2 for H to ~ 1.5 for He and ~ 2.0 for heavy ions. In addition to energy loss, backward electron emission is also dependent on the charge state of the incident ion, so that the mean number of electrons emitted increases by about 10% per charge state [43, 44].

For thin DLC films, electron emission is proportional to the film thickness. According to the literature [45], the secondary electron yield of carbon foils for 12 MeV ^{12}C ions are saturated for a carbon foil thicker than 15 μg/cm^2, whereas for 3 and 10 μg/cm^2 thick foils the electron emission is 65% and 90% of the maximum yield, respectively. In addition to the secondary electron emissions, other factors affect the detection efficiency of the TOF detector. The electrons must pass through wire grids of an electrostatic mirror with a transparency of $\approx 85\%$. Moreover, the electron detection efficiency of the MCP is determined by the probability that an incident electron creates an electron cascade when hitting a channel wall and is given by the sum of two components, namely: the open area and the front surface. For electrons with energies between a few hundred eV and a few thousand eV the MCP quantum efficiency is higher than the active area of the channels and is estimated to be $\approx 76\%$ [46]. The detection efficiency is illustrated in fig. 5 for the ions of four elements.

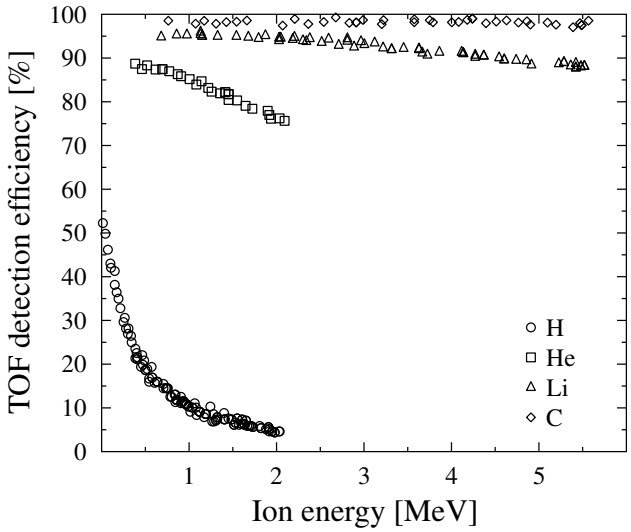

Figure 5: TOF detection efficiency for light recoils as a function of the energy

The coincident detection of the ion velocity and energy produced a histogram such as the one shown in Fig. 6(a), in which the signals generated by different masses lie on different and discrete curves. In this way, each element can be identified and analysed separately. The extracted depth profiles are shown in fig. 6(b).

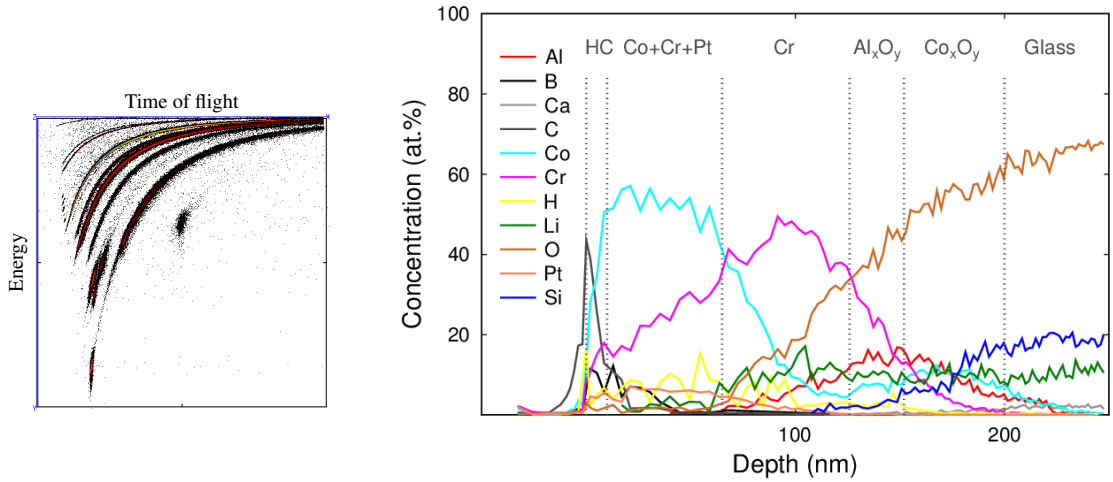

(a) (b)

Figure 6: Ferromagnetic multilayer film of hard disk on a glass substrate measured using a 53 MeV ^{79}Br beam. The time of flight vs energy histogram of the raw data (a) and the corresponding extracted elemental depth profiles (b).

The energy and depth resolution are important factors in the analysis of very thin samples. The use of thin DLC foils in the timing gates reduced the effect of straggling and multiple scattering to the energy resolution. Moreover the quality and homogeneity was better controlled for DLC films than for carbon foils. One of the main contributions to TOF spectra energy resolution is time resolution. The time resolution of TOF comprises two components [47, 48]. The intrinsic time resolution includes the flight time spread of electrons emitted from DLC foils, time delay differences, and the uncertainty due to electronics. The intrinsic time resolution is independent of experimental parameters, including projectile, energy, flight length. Another contribution to time resolution originates from the energy spread, which is related to the ERDA method. The improvements to the time detection electronics (e.g increasing MCPs inter-plate and anode gap voltage, reducing MCP pore size) implemented in this study have improved the intrinsic time resolution to ≈200 ps.

4.1.2 Gas ionisation detector

As a beam dose is often the limiting parameter in the analysis, one needs a detector solid angle that is as large as possible. With a large solid angle, the depth resolution at the surface is dominated by the kinematic energy spread. For example, a typical detector energy resolution of about 1% corresponds to an energy shift generated for example by 10 mrad acceptance angle or by 0.5 msr solid angle at a 40° scattering angle. Therefore good depth resolution and large solid angle are exclusive unless a kinematic energy correction can be performed. Gas ionization detectors can be easily made large and also particle position sensitive: i.e. the scattering angle can be measured simultaneously with the energy and the atomic number of the recoils. At the University of Helsinki, an ionisation counter was built with a solid angle of about 10 msr and an angular resolution of better than 1.5 mrad (fig 7). The detector has a subdivision of the anode for ΔE_1, ΔE_2 and E_{res} measurement, and is shielded from the cathode by a Frisch-grid as shown in fig 8. The anode part ΔE_2 is split into two backgammon shaped halves to produce position information in the scattering plane. In addition, a position signal perpendicular to the scattering plane can be derived from the ratio of the anode and cathode pulse heights. Thus, the detector has position sensitivity in two dimensions. The position signals can be used to correct the measured energy of each recoil event to correspond to the energy calculated for the mean scattering angle [20].

The X-position co-ordinate can be determined since the anode is divided into two equal parts (fig. 8), anode left (AL) and anode right (AR), so that the particle traverses more within the left anode

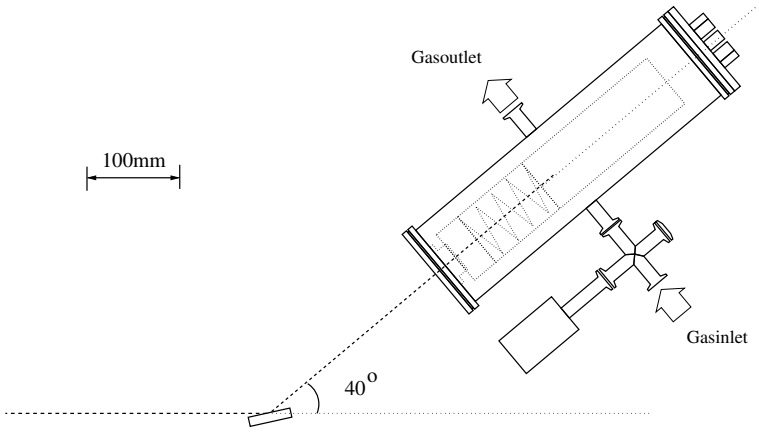

Figure 7: Schema of the gas telescope. Gas inlet and outlet are shown by the arrows.

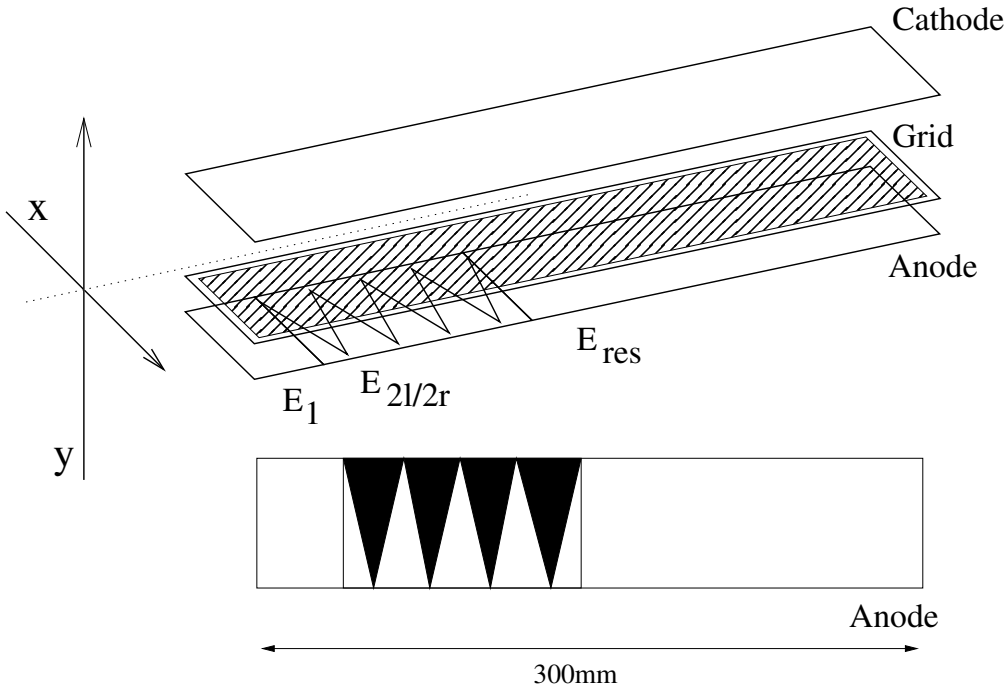

Figure 8: Schematic diagram showing the dimensions of the gas ionisation detector anode and cathode.

when the particle enters from the left side and *vice versa*. The anode part is divided in saw tooth shape as shown in fig. 8 to obtain linear and reliable position co-ordinates. The X-position co-ordinate is obtained from the relation $X = (AL - AR)/(AL + AR)$. Examples of the relation of AL and AR signals are shown in fig. 9.

The cathode signal depends on the position at which the ion pair is formed because no grid is used to screen the ions. However, the total energy of the incident particle can be measured from the anode. Hence the Y-position signal can be directly derived from the cathode signal just by normalising it by the anode signal ($Y = C/E$), as in fig. 9. The position sensitivity of the gas ionisation detector was tested by using a mask with holes in front of the detector. An example of the results of such measurements are shown in figures 9 and 10.

Depending on the particle and its energy the pressure (8–20 mbar) of the isobutane counting gas can be chosen such that the particles stop in the detection volume. Gas pressure is kept constant during measurement by a valve equipped with a microcontroller. The number of ions produced in the gas depends considerably on the particle type and velocity, since the non-ionizing energy loss contribution is substantial for slow ions. Therefore, the electrical signal height produced by an event is not strictly proportional to the residual energy of the particle after passing through the window.

The drawbacks of gas ionisation chambers are the relatively low ionization yield per deposited energy and the requirement that the particles must enter the detector through a thin window, which causes energy loss and straggling. At low particle velocities, a considerable amount of the energy can be lost in the entrance window. For these reasons, the use of gas ionisation detectors below a certain energy limit is excluded. Naturally the detector entrance window has to be as thin and as uniform as possible. Usually, mylar or polypropylene foils with thicknesses between 0.5 and 2 μm are used. Polypropylene (72.5 μg/cm^2) was used as a window material in this study series.

4.2 Analyses

4.2.1 Stopping forces

The most obvious procedure to determine stopping forces is to measure the energy lost by the ions in the transmission through a slab of known thickness. The main complication of this method is the

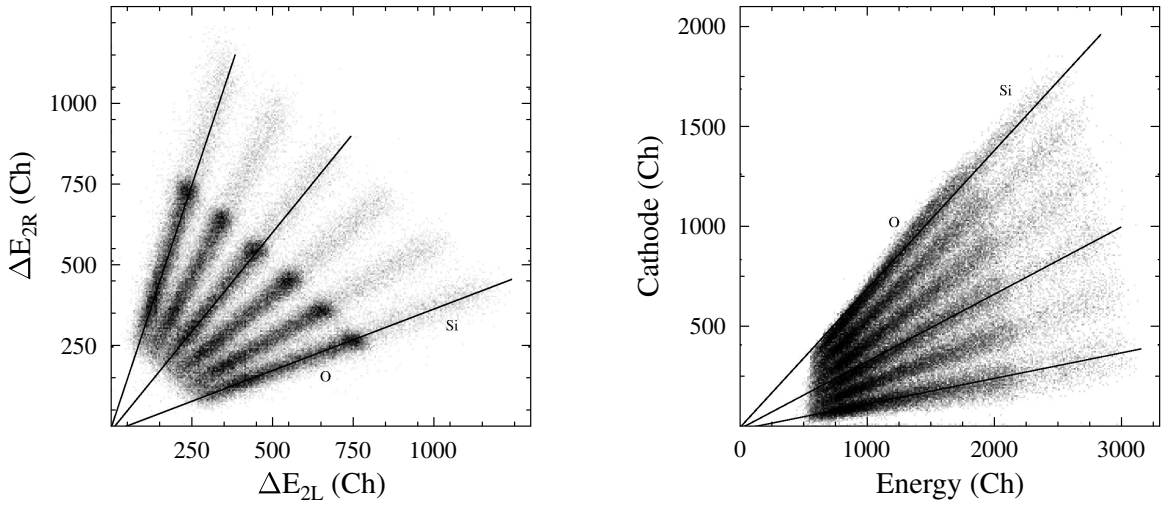

(a) (b)

Figure 9: A SiO_2 sample measured by a gas ionisation detector through a mask with 6×6 holes. The relation of signals from the right and left parts of the anode is shown (a). Cathode signal as the function of energy is plotted (b). Energy units are given in channels

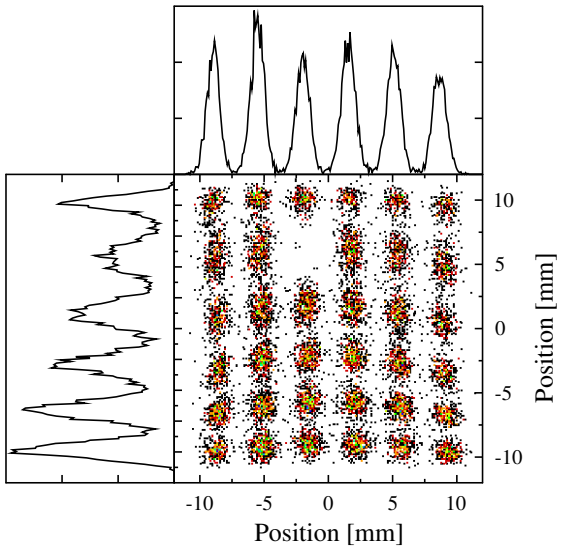

Figure 10: Position spectrum measured through the hole mask. The projections of the X and Y spectra are plotted on the x and y axies.

dependence on thin self-supporting samples, since the beam should not lose more than a few per cent of its energy while traversing through the sample. This restriction imposes tight constraints on the material thickness. Fabrication, handling, and characterisation of such samples impose limits on the available materials. The main source of uncertainty in this method is usually the determination of the thickness (areal density) of the sample foil, in addition to its homogeneity and purity.

The TOF telescopes that are equipped with coincidence setups allow very efficient determinations of the transmission measurements, providing continuous stopping force curves, often for various ions at the same time. Accurate descriptions and results obtained using this method have been published in [49–56]. A general schematic diagram of this type of set-up is shown in figure 11(a).

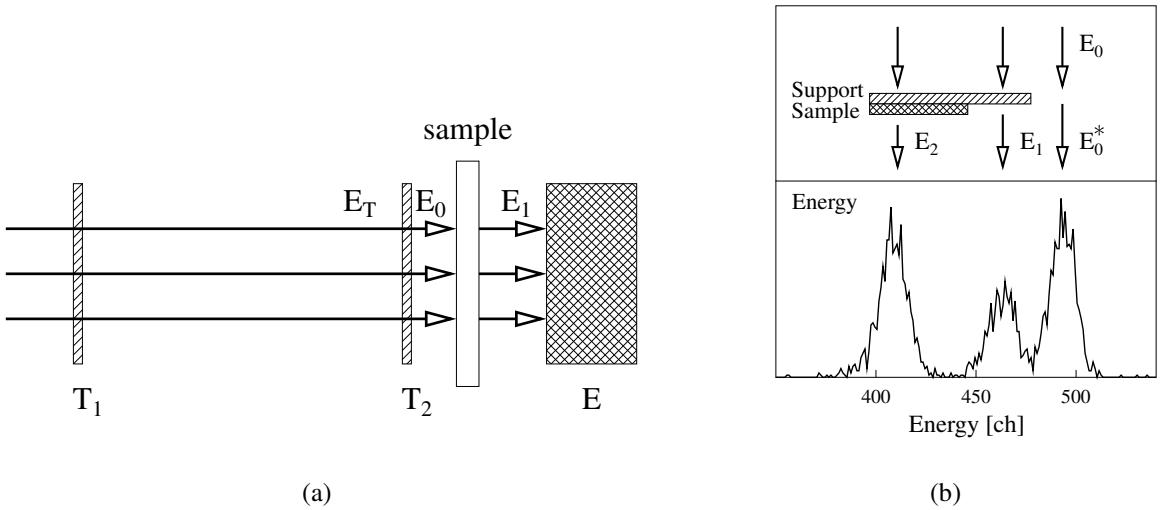

Figure 11: Schematic illustration of a transmission measurement principle (a) and the energy histogram of 10 MeV ^{12}C ions for Ta_2O_5 (b). Data obtained without sample foil (E_0^*) is used to calibrate the energy detector.

In this method the primary beam is used to produce a secondary, less intense beam with a broad energy distribution. The secondary beam can consist of either scattered primary ions or recoils from the scatterer. In both cases, a broad energy distribution can be achieved by using a thick scatterer. The beam is detected by a TOF telescope in which the stopper foil with the material to be studied is inserted between the last time gate and the energy detector. TOF-E two dimensional spectra for the stopper foil and also without it are recorded. The time of flight can be used for tagging the energy of each ion before passing the stopper, hence performing a point-by-point monochromatization of the secondary beam. Moreover, when the secondary beam is composed of different ions, the

discrete TOF-E spectra can be separated, which permits the collection of data for various ions simultaneously.

Measuring the energy differences of the points taken with and without a foil and tagged with the same energy before scattering, allows the energy loss to be obtained for all energies covered by the secondary ion beam. Such measurements are usually performed for heavy ions, which lack stopping force data. Unfortunately, the response of the energy detector is not linear for heavy ions [57–61]. Two approaches are used to overcome this difficulty. Trzaska proposed the use of the TOF system for careful calibration of the energy detector [55], which includes a direct measurement of the pulse height defect (PHD) in the energy detector. Alternatively, Zhang proposed "inverse tagging" of the ion energy before the stopper [62]. This inverse tagging requires using the energy detector to define identical energies, but without actually quantifying these energies and it also relies upon the corresponding time values to obtain the energy values.

The TOF-ERDA setup described in section 4.1.1, was modified for the stopping force measurements. The energy detector was moved backwards allowing the insertion of a sample holder for the stopping foils to be placed between the energy detector and the second timing port. The setup houses a sample holder with positions for up to four samples. This makes it possible to measure energy loss simultaneously for three different samples. Moreover the energy detector can be calibrated accurately from the same HI-ERDA spectrum by comparing the TOF signals and the energy signals obtained without a stopping foil.

The choice of sample materials for study in Papers I and II were motivated by both fundamental and practical reasons. The stopping forces for these compounds hitherto had not been experimentally studied for heavy ions. Oxides such as aluminum oxide and tantalum oxide are of interest, in technology due especially to the optical and electrical properties of these oxides. Thin oxide films can be applied as optical coatings, ion-sensitive membranes in solid-state sensors and as high-κ dielectric materials in gate and storage capacitor structures [8, 63–65]. The ALD method which provides excellent uniformity and thickness control is increasingly used to produce thin oxide films [64]. Silicon nitride is a material with good mechanical and thermal properties in addition to having high chemical stability. Therefore, it is used for protective coatings in some industrial applications such as cutting parts or motor components. Thin self-supporting membranes of Si_3N_4 are also used in research laboratories as vacuum windows or as substrates for microscopy because they are very transparent to radiation and are also mechanically resistant [20, 66]. Polymer films are used in

various ion beam and technical applications such as stopping foils, detector windows, and for the masking of ion beams.

In the measurements made in this present study, heavy ion beams of ^{12}C, ^{16}O, ^{35}Cl, ^{79}Br, and ^{127}I scattered from a heavy element bulk target were used. α-particles from an Am α–source were used to test the setup and the analysis method.

The procedure for extracting the stopping force curves was based on comparing the TOF-E curves obtained with and without the stopper foil. The comparison was made for ions that have the same time value, T_0, and by measuring the difference in the associated E. The energy loss was determined as a function of the initial energy $E_i(T_0)$ in the equation

$$\Delta E = E_i(T_0) - E_f(T_0), \tag{13}$$

where $E_f(T_0)$ is the energy measured after the stopping foil. $E_i(T_0)$ and $E_f(T_0)$ are the energies corresponding to the same time of flight, T_0 for the cases without and with the stopping foil, respectively. Typically the stopping force is calculated as:

$$S(\bar{E}) = \frac{E_i(T_0) - E_f(T_0)}{Nt}, \tag{14}$$

where Nt is thickness of the foil and $\bar{E} = (E_i(T_0) + E_f(T_0))/2$. If the difference between $E_i(T_0)$ and $E_f(T_0)$ was too large, the obtained stopping would be integrated over a too wide an energy range and, therefore, the accuracy would be poorer. Conversely, if the difference was too small, the uncertainties in the energy measurement would also become problematic. The thin foils are better suited for extracting stopping data in the low energy region, where the relative energy loss is larger. The thicker foils are better suited to obtain reliable data at higher energies. In the measurements for the stopping forces, ions should lose roughly between 5% and 50% of their energy due to the stopper foil.

On the other hand, E_f can be calculated by solving the equation

$$\int_{E_i}^{E_f} \frac{dE}{S(E)} = Nt, \tag{15}$$

where $S(E)$ is the stopping force. The thickness of the foil Nt and energies $E_f(T_0)$ and $E_i(T_0)$ were known experimentally. The stopping force $S(E)$ was varied to obtain the best fit to the measured

data. In the data analysis method, the stopping force was a free parameter in the simulation of the measured data. Optimisation was achieved by using an iteration method, which consists of the following four steps: (i) initial guess for the stopping force, (ii) calculation of the energy loss, (iii) comparison with the experimental results, and (iv) corrections to the stopping force. Steps (ii)-(iv) are iterative. The energy loss in step (ii) was calculated numerically solving E_f according to Eq. 15. The calculated energy loss was compared to the experimental energy loss and difference was used as a correction factor for the stopping force. Using equation 15, the effect of the foil thickness in the accuracy of the evaluated stopping force values were smaller than those obtained by using equation 14. En example of results and difference when results are calculated using means and iteration method for He ions are shown in fig.12.

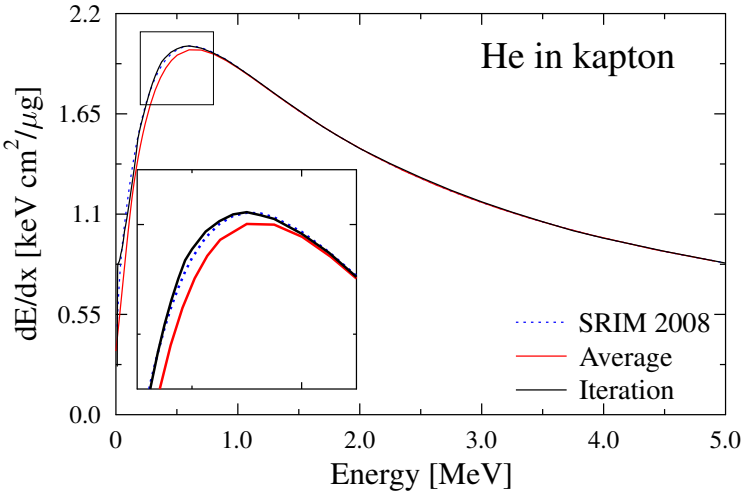

Figure 12: Example of the stopping force calculations and the difference in the results obtained by the mean and iteration methods.

The TOF spectra shown in fig. 13(a) were not ideal due to detector resolution and energy straggling of the ions. Hence, the relation between T and E could not be directly established. The processing of data was needed to obtain an unique curve from the scattered data points before precise calculation of the stopping force. A possible solution can be obtained by using the approach shown in fig. 11. The data are cut in slabs, defined by short time intervals ΔT, given by the TOF system. The data points of each slab are projected onto the energy axis, where the mean or the most probable value, and a value assumed to represent the data for the given interval are obtained.

In a typical spectrum, obtained for heavy ions, the slab energy distributions are not symmetrical and are skewed towards low energy values as seen in fig. 11. In this case, automatic computing of

the mean values of the energy distributions can lead to systematical errors. In most cases, manual inspection allowed fixing the problem simply by filtering or redefining the limits for computation. However, many ($\approx$ 1000) slabs may be taken for each curve, thus it was impossible to perform a manual inspection and make any needed correction in all the cases. In order to reduce the requirements for manual work, "intelligent" algorithms that could discern and identify relevant data from stochastic noise, and automatically set proper filters were used. Algorithms were supported by pre-filtering the data and deleting noise generating events and any artificial structures from the data.

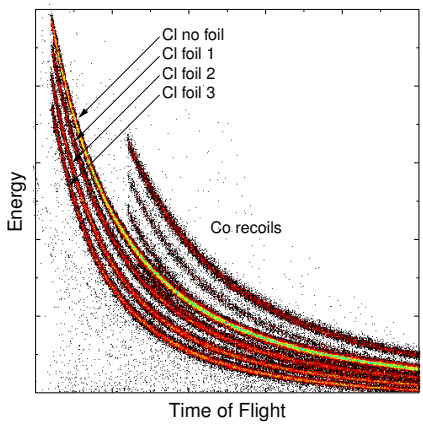

(a)

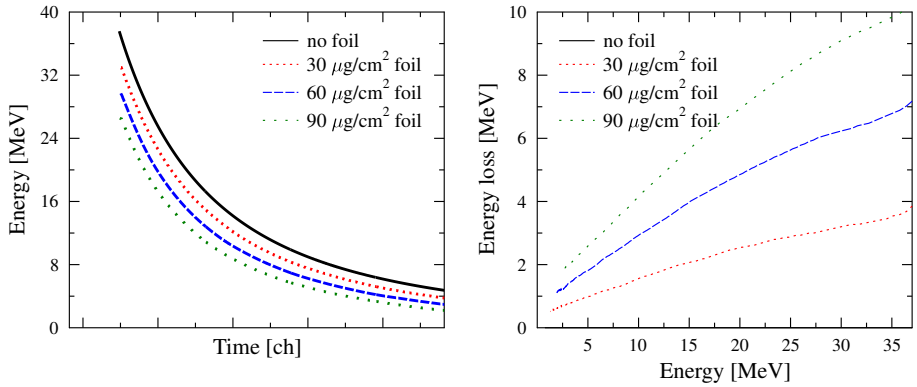

(b)

Figure 13: The TOF-E spectra of stopping measurements and data analysis of 45 MeV Br ions in polyimide (a). In (b) the figure on the left shows averaged data and the figure on the right shows the calculated energy losses for the three different sample thicknesses.

4.2.2 Elemental resolution

The separation of recoil masses can be accomplished by using a TOF system. In a TOF setup both the time of flight along a fixed path and the energy of each recoil are measured. The TOF allows different recoil species with the same energy to be separated, (fig. 14). The mass resolution of the TOF system is given by the time difference at the maximum energy of the recoil elements. The difference in time δt for two elements with masses M_a and M_b is

$$\delta t = 7.1979 \times 10^{-8} l \frac{\sqrt{M_b} - \sqrt{M_a}}{\sqrt{E_b}} = 7.1979 \times 10^{-8} l \left(\frac{M_b}{E}\right)^{1/2} \left[1 - \left(\frac{M_a}{M_b}\right)^{1/2}\right]. \qquad (16)$$

With the energy E in MeV, the mass M in u, and the length l in m, the time δt is in s.

The energy separation of different masses was found to be directly proportional to the incident energy. The mass resolution is limited by the relative energy and velocity resolution

$$\Delta M = \sqrt{\left(\frac{\partial M}{\partial E}\Delta E\right)^2 + \left(\frac{\partial M}{\partial v}\Delta v\right)^2} = M\sqrt{\left(\frac{\Delta E}{E}\right)^2 + \left(2\frac{\Delta v}{v}\right)^2}. \qquad (17)$$

An example of a comparison between a TOF with silicon detector with that of a TOF with gas ionisation detector is shown in fig. 14. Calculated mass resolutions as a function of beam energy for several recoils are shown in fig. 15 (a). The experimental mass resolution in the case of a ^{79}Br beam is shown for several recoil atoms in fig. 15 (b). The mass resolution was obtained by the following procedure. To each detected event a mass m^* is associated, determined by the energy measured with the energy detector and by the velocity measured with the time of flight, according to the relationship $m^* = 2E_{det}/v_{TOF}^2$. For each elemental curve selected from the TOF-E histogram, the mass resolution as a function of energy is calculated by fitting a gaussian curve to the mass distribution, after dividing the events into appropriate energy interval slabs. This procedure requires careful calibration of both the time of flight and the energy detector. A mass resolution (FWHM) better than one atomic mass unit was obtained for elements up to Si using ^{79}Br ions with energies above 30 MeV. At the same incident energy the mass resolution is lower for heavier ion beams, because of the different kinematic factors.

For elements heavier than H, the energy resolution of the energy detector was the dominant factor. The energy resolution of silicon detectors degrades after heavy ion irradiation, therefore the mass

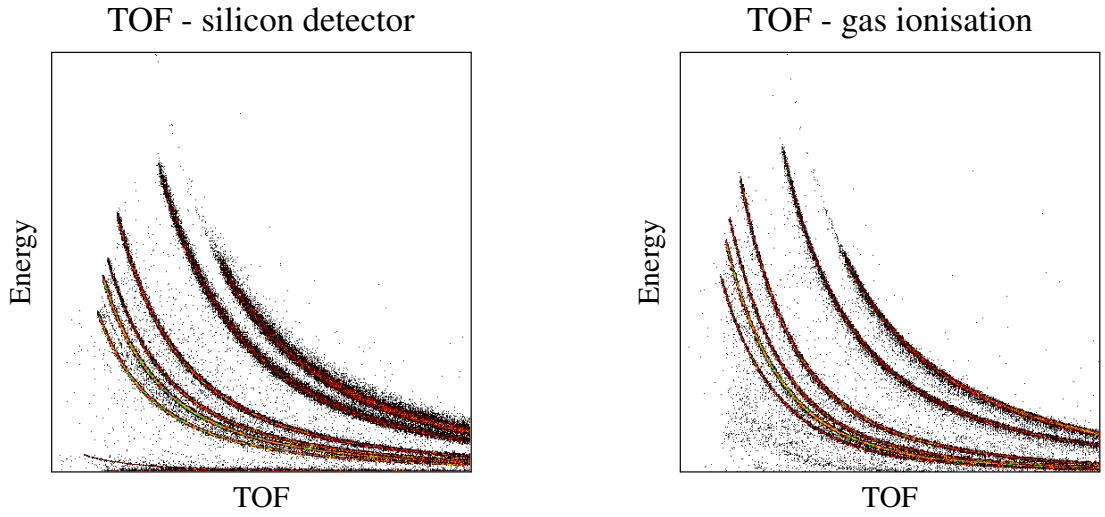

(a) (b)

Figure 14: Raw TOF-E spectra for measurements with 48 MeV ^{79}Br ions. Measurement with a silicon energy detector (a), and with a gas ionisation detector (b). Note the better separation of the heavier elements with the gas ionisation detector.

resolution is related to the status of the detector. This can be overcome by using a gas detector instead of the silicon detectors, as shown by Döbeli *et al.* [67].

The element identification in TOF-ERDA is based on both the velocity and the energy determinations. Another way to separate different recoil species is through their different energy losses in a gas ionisation detector [68]. Gas ionisation detectors require a thin window that separates the vacuum from the gas volume. This causes a significant energy loss and energy straggling, especially for the heavier recoils. For this reason heavy recoils must be rather energetic and therefore gas ionisation detectors are used in the measurements that involve high energy heavy projectiles. The species resolution is obtained by the characteristic differences in the stopping force for different elements.

A detection system is a combination of two detectors namely ΔE and E_{rest} detectors. ΔE is a detector in which the incident particle loses only a very small amount of its energy (ΔE) and passes through it. The particle is then stopped completely within the E_{rest} detector. Separate bands in the spectrum that correspond to different elements can be observed in the graph (E - ΔE spectrum), when ΔE ($= KMZ^2/E$) is plotted as a function of E ($= \Delta E + E_{rest}$) [69] as shown in fig. 16 (a).

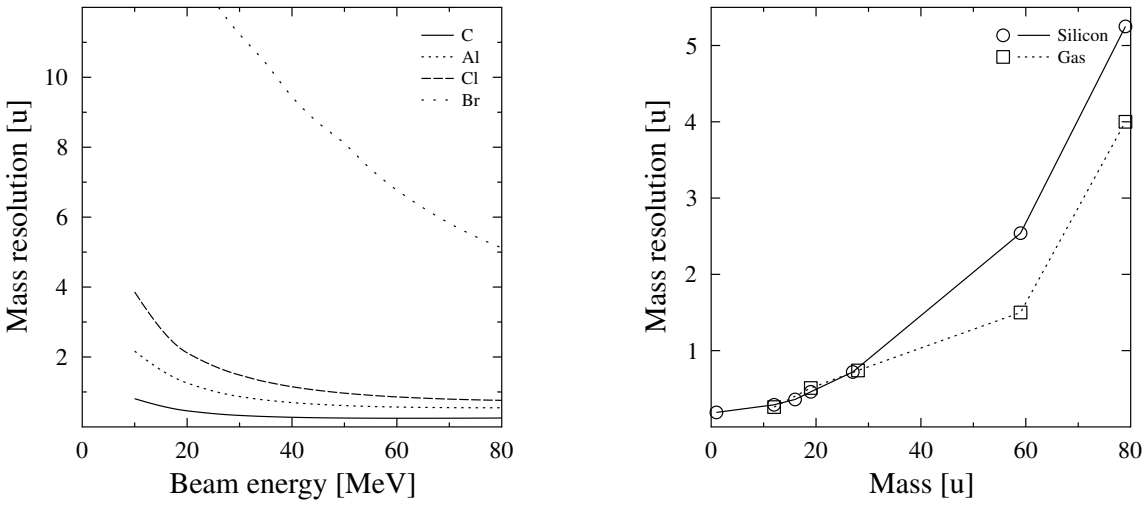

(a) (b)

Figure 15: Mass resolution (FWHM) of the TOF system as a function of ^{79}Br beam energy (a). Comparison of mass resolutions for TOF+ion implanted silicon detector and TOF+gas ionisation detector systems measured with 48 MeV ^{79}Br beam (b).

In an ionisation chamber these features are obtained simply by dividing the anode into two parts [15, 68, 70–76]. In this study the anode length was split into three parts, as shown in fig. 8, to achieve flexibility for the effective lengths of the ΔE and E_{rest} anodes, as shown in fig 16 (b).

4.2.3 Depth resolution

The surface depth resolution is limited by several factors that affect the surface recoil energy inaccuracy. One of these is the beam spot size that causing recoil detection angular differences, when the detector is placed at a finite distance. Beam divergence leads to kinematic energy differences.

Recoils detected at slightly different detection angles have large kinematic energy differences. Usually these kinematic energy differences are reduced by simply restricting the angular acceptance of the recoil detector. An alternative approach is to detect the recoil angle by a position sensitive detector. The effect of the kinematic broadening can be expressed as

$$\Delta E(\theta) = E_0 K_r \frac{2\sin\theta}{\cos\theta}\Delta\theta, \tag{18}$$

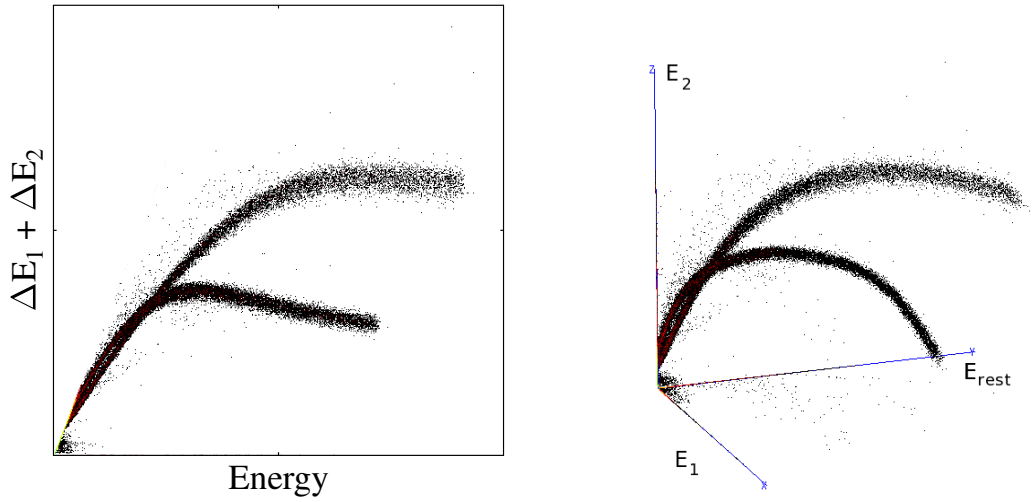

(a) (b)

Figure 16: Measured spectrum of an Al_2O_3 sample obtained by the gas ionisation detector. In (a) ΔE_{1+2} is plotted as a function of E. The relation of signals from the anode parts ΔE_1, ΔE_2, and E_{rest} in the three dimensional plot are shown in (b).

where E_0 is energy of the incident ion, K_r the recoil kinematic factor and θ is the recoil angle. $\Delta\theta$ is the deviation of the recoil angle.

Other significant factors that affect the depth resolution are the timing resolution, TOF length uncertainty, and a possible non-homogeneity of the timing DLC foils that causes energy straggling. The contribution of the timing resolution Δt to energy resolution is

$$\Delta E(t) = \frac{M_r l^2}{t^3}\Delta t, \tag{19}$$

where M_r is the recoil mass, l flight path length, and t time of flight. The timing resolution of TOF system is about 200 ps in all cases [17]. The contribution of the TOF length uncertainty Δl is

$$\Delta E(l) = \frac{Ml}{t^2}\Delta l. \tag{20}$$

Energy straggling due to the DLC foil, according to Bohr's simple energy independent expression, is

$$\Delta E(\Omega_B) = 2.35[4\pi(Z_1 e^2)^2 N Z_2 \cdot x_C]^{0.5}, \tag{21}$$

where x_C is the thickness of the DLC foil and N DLC foil's atomic density. DLC foil non-homogeneity Δx_C contributes to the energy resolution as

$$\Delta E(x_C) = \frac{dE}{dx}|_C \cdot x_C \cdot \Delta x_C. \tag{22}$$

The incident beam energy spread component due to accelerator ripple is less than 0.1%. Moreover the tandem effect component that indicates the change of the ion charge state in the first carbon foil that results in a small acceleration or deceleration is also negligible.

The position sensitive detector allows the position signals to be used to correct the measured energy of each recoil event so that it corresponds to the energy calculated for the mean scattering angle.

The experimental energy resolution can be extracted by fitting an error function to the high energy edges of the energy spectra. The conversion to depth can be obtained by using the surface approximation [77]. The surface depth resolution and all contributors are shown in fig.17.

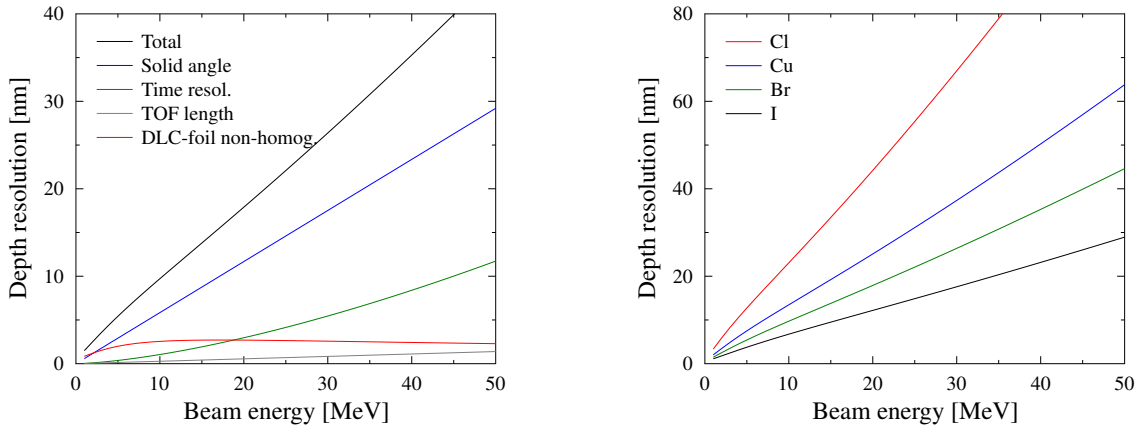

(a) (b)

Figure 17: Surface depth resolution as a function of the beam energy. The O atoms were recoiled by a ^{79}Br beam incident on a Al_2O_3 layer (a). The total depth resolutions at the surface for different incident ions as a function of the beam energy, are shown in (b).

The experimental depth resolution below the surface can be ascertained by determining the energy resolution at the interface of the sample layers. Similar treatments can be used as in the case of the surface depth resolution, but the energy loss of the incident ion in the sample has to be considered. Simulations can be performed using Monte Carlo codes to study the depth resolution below the

surface. All experimental parameters of the detector set up in addition to multiple scattering and straggling in the sample layer can be included in the simulations. The depth resolution at all depths can be extracted easily from the output of the simulations by dividing the TOF resolution by the deviation in the detected time of flights of particles originating from a specified depth.

The main limiting factors of the ERDA surface depth resolution are the detection solid angle and the timing resolution. The best resolution can be achieved in the low energy limit. The use of heavier ions with increasing energy gives a better surface resolution. Depth resolution deeper in the sample is dominated by multiple and plural scattering. These two phenomena increase when the incident beam mass increases or the energy decreases. Depending on the film thickness, a compromise between energy and ion species must be made to achieve a good resolution through the sample film. The use of small incident angles may also improve the depth resolution, but the drawbacks are the same as for thick samples.

4.2.4 Calibration

The timing resolution is mainly determined by the intrinsic properties of the timing gates, i.e. the quality of the output signal from the anode and the differences in the electron path lengths. The effect of the latter is negligible in the timing gate design used in this study, as the electrons emitted from different parts of the carbon foils undergo similar path lengths in the electrostatic mirror.

Accurate measurement of the timing resolution is not a straightforward task. A typical procedure to measure it is to observe the high-energy edge of the signal from scattered primary particles or recoiled atoms, as in such cases, other effects can be often neglected. However, special attention should be paid to sample selection, especially to surface roughness and isotopic effects.

The energy deduced from TOF has better resolution than that of the energy detector in most cases. The time calibration is also linear for all ions. Consequently, TOF can be used to calibrate energy detectors. TOF is also used to calibrate the solid state energy detector in the stopping force measurements. The energy loss in the second timing gate must be take into account. The energy calibration of the gas ionisation detector was achieved in the same way. The energy loss in the detector window was also considered.

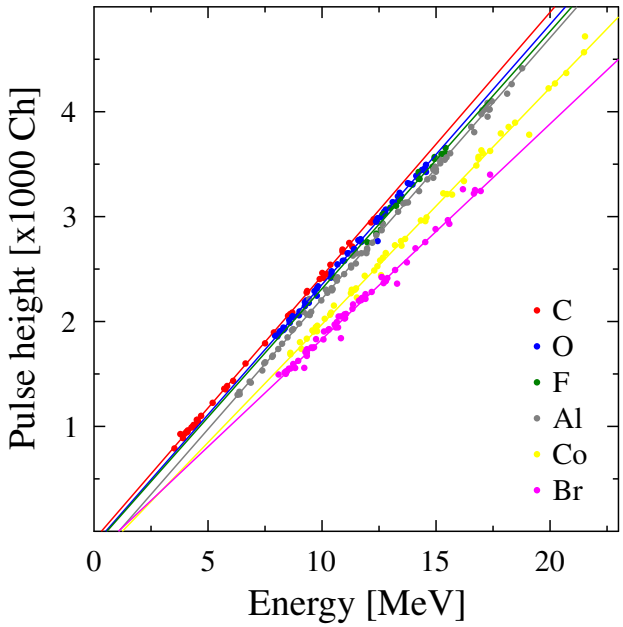

Figure 18: Energy calibration of the gas ionisation detector for different ions.

4.3 Concentration distributions

In IBA, a computer aided data analysis is used to extract information from the measured spectra. The desired information includes identification of sample elements, their concentrations, areal densities and layer thicknesses. In the best case, the spectrum can be converted into concentration depth distributions of all elements in the sample.

The calculation methods can be divided into two types namely: the direct calculations and simulations. In direct spectrum analysis, the yields from separated spectrum signals are transformed into concentration values by closed-form analytical calculations. Another form of direct analysis includes conversion from signal areas and heights into total amounts or concentrations. This is the opposite of spectrum simulation, whereby a theoretical spectrum is generated from an assumed depth profile that is then compared with the actual data.

The simulation modeling assumes that the underlying physics, mathematics, data (nuclear and atomic) are valid and adequately describe the physical processes involved. Starting from a known sample structure, the corresponding experimental energy spectrum can be simulated by applying

basic data and the known formalism of the reaction mechanism. By comparing the experimental and theoretical spectra and iteratively modifying the assumed sample composition, a close similarity to the spectra is typically attained after only a few iterations. The sample structure that most closely lead to the theoretical spectrum is then adopted to correspond to the sample structure.

A typical simulation process has four steps.

1. An initial sample composition is assumed.
2. A theoretical spectrum that corresponds to the experimental parameters and the assumed sample composition is calculated.
3. The simulated spectrum is compared to the experimental spectrum.
4. Differences are identified and the assumed sample composition is modified accordingly.

These iteration steps are repeated until a good fit between the simulated and experimental spectrum is obtained. In the simulations, the sample is divided into thin sublayers. The incoming beam energy and the detected energy for scattering for each element are calculated for each layer. The simulated spectrum is then constructed based on these quantities and also on the concentration of the element in each sublayer. Straggling and other physical phenomena can be included, and these are usually treated statistically. Individual collisions between the analysing ion and the target nuclei and their associated electrons are not modelled. Monte Carlo simulations model individual interactions between particles. In this way, phenomena that have usually been difficult to include in the standard conventional method are easily included.

The standard methods face problems in the analysis of heavy-ion TOF-ERDA data, particularly at low energies in which multiple scattering plays a very important role. Not only are the signals broadened, but also the actual yield is not what would be expected from single scattering. In practice, ion–electron interactions are not calculated, and tabulated stopping forces are used. Nevertheless, complex physical processes such as double and multiple scattering, in addition to the full ion–detection system interaction, are taken into account in codes such as MCERD and Corteo [33, 34].

4.4 Surface roughness and structures

Samples in ion beam analysis are usually assumed to have smooth surfaces, e.g. thin layers deposited on Si wafers or glass substrates. It was recognized very early using RBS, that surfaces roughness can strongly influence the shape of the measured energy spectra [78]. ERDA is very sensitive to surface roughness, because of the oblique scattering geometry [74]: particularly with heavy ion projectiles.

The difference between rough and smooth surfaces in analysis is how the effective path length of the projectiles and ejecting recoils, i.e. the ion track inside the sample is determined. Particles can also exit the sample material one or more times depending on the incident and exit angles and the surface structure properties. Another difference compared to a smooth surface simulation is the step width that is used in the programs to calculate the energy and cross-sections related to a scattering event.

Monte Carlo programs that have been specially developed to simulate ERDA measurements allow the proper treatment of surface roughness [79]. The simulation programs can use 3D surface structures in the calculations.

ERDA is conventionally used to analyse thin film materials. Novel materials and more complex devices and structures impose new challenges to IBA techniques. IBA is a stand alone technique and provides all information from elemental compositions to depth profiles for thin film analysis. However, IBA methods can also complement other characterisation procedures for the analyses of more complex structures.

The concentration analysis of the commercial solar thermal absorber coatings was reported by the author and others in ref. [7]. Coatings were applied onto copper and aluminium substrates. Copper and aluminium substrates were typical cold-rolled products. Substrate surface roughness and striations from rolling process or other defects of the substrate material influenced the microstructure of the coating. After the ageing treatment, diffused islands were observed from the surface of absorbers with copper substrates along the direction of rolling as shown in figure 19. Microstructural analyses of the thermal absorber samples were performed by ultra-high resolution field-emission scanning electron microscope (FESEM).

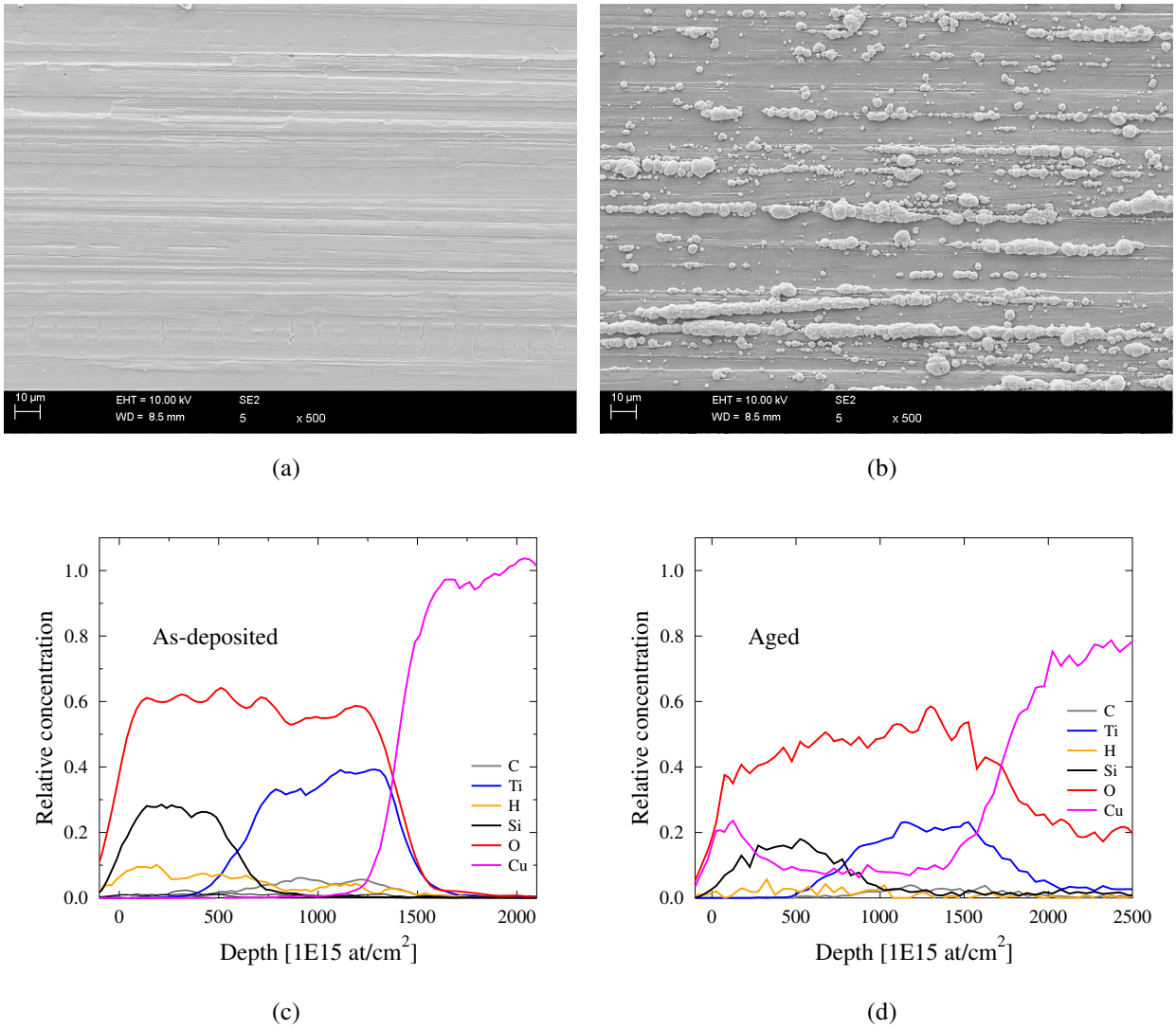

Figure 19: FESEM images of titanium oxy-nitride coatings on copper as-deposited (a) and aged (b). The rolling direction of the substrate is seen as horizontal striations in the pictures. Islands of oxidized copper were created along rolling scratches of the substrate during the ageing.TOF-ERDA depth profiles of the titanium oxy-nitride samples. The copper substrate has oxidised and copper has diffused to the sample film.

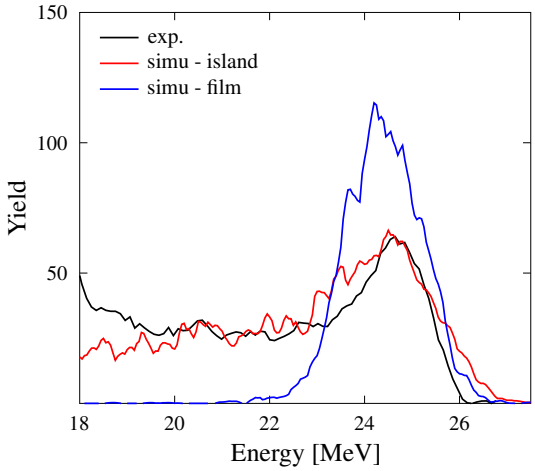

Figure 20: TOF-ERDA energy spectra and MC simulations of copper islands on the chromium oxy-nitride samples. Thin homogeneous Cu film is also simulated for comparison.

In figure 19, the effect of the surface structure was not taken in the account. However, the energy spectrum of the copper was simulated using MCERD program to analyse the amount of copper inside of the thermal absorber film. The effect of the result of the analysis is shown in fig. 20. The difference in the results shows that to obtain the correct result the surface structure must be taken account. Samples with Au- and Si-nanocystals were analysed similarly in paper IV and in ref. [6].

4.5 Ion beam induced modification

IBA methods are usually considered as non-destructive. The reason is that they do not create macroscopic and visible damage to the measured sample, such as that encountered by sputtering based methods. However, the interaction between the incident ions and the target atoms does introduce sample modifications. The interaction between nuclei that are responsible for the recoil formation displaces atoms inside the film. The interaction with the atoms' electrons that are responsible for the ion slowing down affects the electric and chemical state of the sample atoms. Scattering cross-sections for the recoils in case of heavy ion ERDA are proportional to $(M_i Z_i)^2$. This strong Z_i dependence allows ERDA to be performed using quite low beam fluence. TOF-ERDA systems typically require larger ion fluence than for example gas ionisation systems due to the small solid angle of the detector. In addition, electronic stopping forces increases roughly linearly with Z_i, therefore

the sample damage caused during analysis using heavy ions should be less than that created during ERDA using light ions. The beam fluence in ERDA is typically in the order of 10^{12} ions/cm^2 and the number of target atoms actually involved in collision processes is only a small fraction of the total.

Desorption of the atoms of light sample elements was observed during irradiation of thin ALD crown TaO - polyimide multilayer samples with a 43 MeV ^{79}Br beam. The fast loss of elements is followed by a stable phase as shown in the fig. 21. Elemental losses occur, even when the effect is more limited to low beam energies. Decrease of the element concentration can be fitted by an exponential function of the ion fluence Φ which enables correction of the analysis result.

In the case of typical ALD samples, the irradiation-induced damage can be neglected most of the times, but the possible changes in the sample composition had to be routinely monitored.

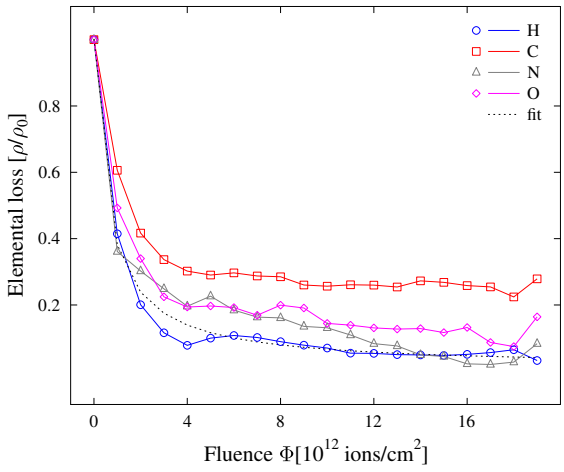

Figure 21: Loss of H, C, N, and O from polymer film during irradiation.

Along with the plot of the actual experimental data there is also a fitted function to the H data according to the equation

$$\rho(\Phi) = \frac{1}{\frac{1}{\rho_f} + (\frac{1}{\rho_0} - \frac{1}{\rho_f})e^{-K\Phi}}, \tag{23}$$

where ρ_f and ρ_0 are the final and initial concentration and K is the release cross section. The equation introduced by Adel et al. [80] is based on the statistical model on bulk molecular recombination and is valid for hydrogen loss. The model assumes that H radicals are formed and they recombine into H_2 molecules, which are able to diffuse out of the sample.

5 Conclusions and outlook

This study describes the progress achieved in the development of heavy ion ERDA.

The detectors used were characterised in terms of timing resolution, energy resolution, detection efficiency and mass resolution. The improved timing resolution of the TOF detector achieved that was enabled a mass resolution that was better than 1 u for elements lighter than Si. The system demonstrated high quantification accuracy and reproducibility, in terms of both film composition and thickness. In most of the cases considered, the measured standard deviation was less than 5%.

The position sensitive gas ionisation detector for heavy ion ERDA was installed and tested. Energy calibration curves and energy resolution of the ionisation chamber were measured for several ions by coupling the gas detector to the TOF system. Identification of all ions within single measurement was achieved. The detector had an energy resolution of 0.5 % for light ions and about 1.5 % for Si ions within the energy range used in ERDA. The detector design used provided data on position independent of particle and energy with a position resolution that was better than 0.5 mm.

A TOF system combined with either a silicon detector or a gas ionisation detector, provided an energy resolution from a time measurement that was usually better than that of the energy detector. Performance of the gas ionisation detector was found to be better than that of the ion implanted silicon detector for almost all ions. Nevertheless, the analysis of typical thin ALD samples revealed that the use of the silicon detector for element separation in a TOF system is sufficient and is also easier to use. When the separation of heavy recoils are required, gas ionisation detector is the better choice. For heavy ions the improvement in energy resolution was more than a factor 2. The use of a gas ionisation detector as energy detector in TOF-ERDA improved the particle identification for ERDA. In contrast to solid state detectors, gas ionisation detectors are not prone to radiation damage, and have energy resolution of the order of 1%.

Monte Carlo simulations with MCERD and Corteo programs were run in the analysis procedure to complement the standard analysis in order to increase the quantification accuracy for films less than 10 nm thick, and for materials with rough surfaces (also nano particles and small structures). Tests carried out on challenging materials showed a high sensitivity of the simulation code to small variations of both film composition and thickness.

The data and analysis result storage system based on sql database was developed to facilitate measurement data handling. Fast access to all measured data and results allows an easy approach to compare results and to monitor detector parameter trends.

The damage induced on the sample material caused by the beam irradiation was studied. Results show significant elemental losses during analysis particularly when measuring polymer samples. Detection systems with large solid angles reduce damage creation, as they require lower ion fluence. The use of heavy ions and high energies can reduce damage production e.g. in case of polymer samples.

The stopping force values for important industrial materials and ions most frequently used in HI-ERDA have been obtained. A clear advantage of using the studied procedure compared to conventional measurements methods was that the uncertainty connected to the estimation of the ion mean energy in the sample foil is avoided.

The improved ERDA capabilities studies will be exploited in the characterisation of atomic layer deposited structures provided through the Finnish Centre of Excellence in Atomic Layer Deposition of which our laboratory is a partner. The samples to be studied consist of thin films, micro- and nanostructures, materials for microelectronics and energy technologies.

ACKNOWLEDGEMENTS

I wish to thank my supervisor the head of the Department of Physics at the University of Helsinki, Professor Juhani Keinonen, and the head of the Division of Materials Physics, Professor Jyrki Räisänen, for giving me the opportunity to work in the accelerator laboratory and for providing the facilities for my research. Without your support during this long time this theses would not have been completed.

I would also like to thank Dr. Kai Arstila, Docent Timo Sajavaara and Docent Eero Rauhala for introducing me to the interesting world of ion beam analysis and accelerator technology. I was very lucky to get a chance to learn experimental techniques and skills directly from such experts.

I am also highly indebted to Docent Pertti Tikkanen for his professional guidance and all the help I received from him over the years. Without Pertti I would have been helpless with the accelerators, vacuum systems and other technical practicalities. I am also indebted to the operators of the accelerator, especially Pietari Kienanen, for keeping the accelerators running and producing the ion beams for me to measure. I am also thankful to all the technical personnel, especially Pasi Siiki and Sisko Vikberg and our secretaries Tuire Savolainen and Tiina Hasari for all their help.

I thank my co-authors who have collaborated in these publications. I would also like to thank all my colleagues, who have created a fruitful and most efficient atmosphere for working in the laboratory. Special thanks are also due to Drs. Kalle Heinola, Vesa Palonen, Tommy Ahlgren, Samuli Väyrynen and M.Sc Risto Jokinen for interesting and stimulating conversations about physics in addition to other things.

I also thank my friends, especially Kimmo Hoikka and Mikko Loikkanen, and all the other people who have closely followed this process for their presence, support and encouragement. They are too many to mention by name but they know who they are.

I want to thank my parents, sister, and brother for everything. My warmest thanks go to my sons, Pessi and Nuuti, who have been the lights of my life and for reminding me of the true priorities of life. Finally I would like to thank Katja for her loving presence and patience during all of this work.

Financial support from the Magnus Ehrnrooth foundation and Faculty of Science at University of Helsinki is gratefully acknowledged.

Helsinki, November 2012

K. M.

References

[1] J. Tesmer, M. Nastasi, J. C. Barbour, C. J. Maggiore, and J. W. Mayer, *Handbook of modern ion beam materials analysis* (Materials Research society, Pittsburgh, 1995).

[2] J. L'Ecuyer, *An accurate and sensitive method for the determination of the depth distribution of light elements in heavy materials*, J. Appl. Phys. **47**, 381 (1976).

[3] W. M. A. Bik and F. H. P. M. Habraken, *Elastic recoil detection*, Reports on Progress in Physics **56**, 859 (1993).

[4] R. Groleau, S. Gujrathi, and J. Martin, *Time-of-flight system for profiling recoiled light elements*, Nuclear Instruments and Methods in Physics Research **218**, 11 (1983).

[5] J. Thomas, M. Fallavier, D. Ramdane, N. Chevarier, and A. Chevarier, *High resolution depth profiling of light elements in high atomic mass materials*, Nuclear Instruments and Methods in Physics Research **218**, 125 (1983).

[6] L. Costelle, A. Pirojenko, V. Tuboltsev, A. Savin, K. Mizohata, and J. Räisäinen, *Spin-glass magnetism of surface rich Au cluster film*, Appl. Phys. Lett. **99**, 022503 (2011).

[7] M. Kotilainen, K. Mizohata, M. Honkanen, and P. Vuoristo, *Influence of microstructure on temperature-induced ageing mechanisms of different solar absorber coatings*, Solar Energy Materials and Solar Cells (submitted for publication).

[8] C. L. Dezelah, M. K. Wiedmann, K. Mizohata, R. J. Baird, L. Niinistö, and C. H. Winter, *A pyrazolate-based metalorganic tantalum precursor that exhibits high thermal stability and its use in the atomic layer deposition of ta(2)o(5).*, J. Am. Chem. Soc. **129**, 12370 (2007).

[9] J. Niinistö, T. Hatanpää, M. Kariniemi, M. Mäntymäki, L. Costelle, K. Mizohata, K. Kukli, M. Ritala, and M. Leskelä, *Cycloheptatrienyl-Cyclopentadienyl Heteroleptic Precursors for Atomic Layer Deposition of Group 4 Oxide Thin Films*, Chem. Mater. **24**, 2002 (2012).

[10] V. Pore, K. Knapas, T. Hatanpää, T. Sarnet, M. Kemell, M. Ritala, M. Leskelä, and K. Mizohata, *Atomic Layer Deposition of Antimony and its Compounds Using Dechlorosilylation Reactions of Tris(triethylsilyl)antimony*, Chem. Mater. **23**, 247 (2011).

[11] J. Likonen, A. Hakola, J. Strachan, J. Coad, A. Widdowson, S. Koivuranta, D. Hole, K. Mizohata, M. Rubel, S. Jachmich, and M. Stamp, *Deposition of 13C tracer in the JET MkII-HD divertor*, J. Nucl. Mater. **415**, S250 (2011).

[12] M. Bosund, K. Mizohata, T. Hakkarainen, M. Putkonen, M. Söderlund, S. Honkanen, and H. Lipsanen, *Atomic layer deposition of ytterbium oxide using -diketonate and ozone precursors*, Appl. Surf. Sci. **256**, 847 (2009).

[13] P. Goppelt, B. Gebauer, D. Fink, M. Wilpert, T. Wilpert, and W. Bohne, *High energy ERDA with very heavy ions using mass and energy dispersive spectrometry*, Nucl. Instrum. Methods Phys. Res., Sect. B **68**, 235 (1992).

[14] G. Dollinger, *Elastic recoil detection analysis with atomic depth resolution*, Nucl. Instrum. Methods Phys. Res., Sect. B **79**, 513 (1993).

[15] W. Assmann, H. Huber, C. Steinhausen, M. Dobler, H. Glückler, and A. Weidinger, *Elastic recoil detection analysis with heavy ions*, Nucl. Instrum. Methods Phys. Res., Sect. B **89**, 131 (1994).

[16] R. Siegele, H. K. Haugen, J. A. Davies, J. S. Forster, and H. R. Andrews, *Forward elastic recoil measurements using heavy ions*, J. Appl. Phys. **76**, 4524 (1994).

[17] J. Jokinen, J. Keinonen, P. Tikkanen, A. Kuronen, T. Ahlgren, and K. Nordlund, *Comparison of TOF-ERDA and nuclear resonance reaction techniques for range profile measurements of keV energy implants*, Nucl. Instrum. Methods Phys. Res., Sect. B **119**, 533 (1996).

[18] T. Winzell, Y. Zhang, and H. J. Whitlow, *Analysis of ferromagnetic removable hard disc media ageing by time of flight-energy elastic recoil detection analysis*, Nucl. Instrum. Methods Phys. Res., Sect. B **161-163**, 558 (2000).

[19] D. K. Avasthi and W. Assmann, *ERDA with swift heavy ions for materials characterization*, Current Science **80**, 1532 (2001).

[20] M. Döbeli, C. Kottler, M. Stocker, S. Weinmann, H.-A. Synal, M. Grajcar, and M. Suter, *Gas ionization chambers with silicon nitride windows for the detection and identification of low energy ions*, Nucl. Instrum. Methods Phys. Res., Sect. B **219-220**, 415 (2004).

[21] Z. Siketic, I. B. Radovic, M. Jaksic, and N. Skukan, *Time of flight elastic recoil detection analysis with a position sensitive detector.*, The Review of scientific instruments **81**, 033305 (2010).

[22] M. Bozoian, K. M. Hubbard, and M. Nastasi, *Deviations from Rutherford-scattering cross sections*, Nucl. Instrum. Methods Phys. Res., Sect. B **51**, 311 (1990).

[23] W. H. Bragg and R. D. Kleeman, *On the alpha particles of radium, and their loss of range in passing through various atoms and molecules*, Philos. Mag. **10**, 318 (1905).

[24] P. Sigmund, *Kinetic theory of particle stopping in a medium with internal motion*, Phys. Rev. A **26**, 2497 (1982).

[25] J. R. Sabin and J. Oddershede, *Theoretical stopping cross sections of C-H, C-C and C=C bonds for swift protons*, Nucl. Instrum. Methods Phys. Res., Sect. B **27**, 280 (1987).

[26] J. Oddershede and J. R. Sabin, *Bragg rule additivity of bond stopping cross sections*, Nucl. Instrum. Methods Phys. Res., Sect. B **42**, 7 (1989).

[27] G. Both, R. Krotz, K. Lohmer, and W. Neuwirth, *Density dependence of stopping cross sections measured in liquid ethane*, Phys. Rev. A **28**, 3212 (1983).

[28] W. K. Chu, *Calculation of energy straggling for protons and helium ions*, Phys. Rev. A **13**, 2057 (1976).

[29] P. Sigmund, *Statistical theory of charged-particle stopping and straggling in the presence of charge exchange*, Nucl. Instrum. Methods Phys. Res., Sect. B **69**, 113 (1992).

[30] Q. Yang, D. O'Connor, and Z. Wang, *Empirical formulae for energy loss straggling of ions in matter*, Nucl. Instrum. Methods Phys. Res., Sect. B **61**, 149 (1991).

[31] E. Szilágyi, *Energy spread in ion beam analysis*, Nucl. Instrum. Methods Phys. Res., Sect. B **161-163**, 37 (2000).

[32] G. Amsel, G. Battistig, and A. L'Hoir, *Small angle multiple scattering of fast ions, physics, stochastic theory and numerical calculations*, Nucl. Instrum. Methods Phys. Res., Sect. B **201**, 325 (2003).

[33] K. Arstila, T. Sajavaara, and J. Keinonen, *Monte Carlo simulation of multiple and plural scattering in elastic recoil detection*, Nucl. Instrum. Methods Phys. Res., Sect. B **174**, 163 (2001).

[34] F. Schiettekatte, *Fast Monte Carlo for ion beam analysis simulations*, Nucl. Instrum. Methods Phys. Res., Sect. B **266**, 1880 (2008).

[35] K. Arstila, J. Knapp, K. Nordlund, and B. Doyle, *Monte Carlo simulations of multiple scattering effects in ERD measurements*, Nucl. Instrum. Methods Phys. Res., Sect. B **219-220**, 1058 (2004).

[36] M. Mayer, K. Arstila, K. Nordlund, E. Edelmann, and J. Keinonen, *Multiple scattering of MeV ions: Comparison between the analytical theory and Monte-Carlo and molecular dynamics simulations*, Nucl. Instrum. Methods Phys. Res., Sect. B **249**, 823 (2006).

[37] J. Jokinen, *Time-of-flight Spectrometry of Recoiled Atoms in the Analysis of Thin Films*, *Acta polytechnica Scandinavica. Ph, Applied physics series* (Finnish Academy of Technology, Espoo, 1997).

[38] Y. Zhang, H. J. Whitlow, T. Winzell, I. F. Bubb, T. Sajavaara, K. Arstila, and J. Keinonen, *Detection efficiency of time-of-flight energy elastic recoil detection analysis systems*, Nucl. Instrum. Methods Phys. Res., Sect. B **149**, 477 (1999).

[39] H. J. Whitlow, G. Possnert, and C. Petersson, *Quantitative mass and energy dispersive elastic recoil spectrometry: Resolution and efficiency considerations*, Nucl. Instrum. Methods Phys. Res., Sect. B **27**, 448 (1987).

[40] R. A. Weller, J. H. Arps, D. Pedersen, and M. H. Mendenhall, *A model of the intrinsic efficiency of a time-of-flight spectrometer for keV ions*, Nucl. Instrum. Methods Phys. Res., Sect. A **353**, 579 (1994).

[41] E. Sternglass, *Theory of Secondary Electron Emission by High-Speed Ions*, Phys. Rev. **108**, 1 (1957).

[42] H. Rothard, K. Kroneberger, A. Clouvas, E. Veje, P. Lorenzen, N. Keller, J. Kemmler, W. Meckbach, and K.-O. Groeneveld, *Secondary-electron yields from thin foils: A possible probe for the electronic stopping power of heavy ions*, Phys. Rev. A **41**, 2521 (1990).

[43] A. Clouvas, C. Potiriadis, H. Rothard, D. Hofmann, R. Wünsch, K. O. Groeneveld, A. Katsanos, and A. C. Xenoulis, *Role of projectile electrons in secondary electron emission from solid surfaces under fast-ion bombardment*, Phys. Rev. B **55**, 12086 (1997).

[44] N. Pauly, A. Dubus, M. Rösler, H. Rothard, A. Clouvas, and C. Potiriadis, *Electron emission induced by H+ and H0 incident on thin carbon foils: influence of charge changing processes*, Nucl. Instrum. Methods Phys. Res., Sect. B **230**, 460 (2005).

[45] P. Koschar, K. Kroneberger, A. Clouvas, M. Burkhard, W. Meckbach, O. Heil, J. Kemmler, H. Rothard, K. Groeneveld, R. Schramm, and H.-D. Betz, *Secondary-electron yield as a probe of preequilibrium stopping power of heavy ions colliding with solids*, Phys. Rev. A **40**, 3632 (1989).

[46] G. Fraser, *The electron detection efficiency of microchannel plates*, Nuclear Instruments and Methods in Physics Research **206**, 445 (1983).

[47] H. J. Whitlow, C. S. Petersson, K. J. Reeson, and P. L. F. Hemment, *Mass-dispersive recoil spectrometry studies of oxygen and nitrogen redistribution in ion-beam-synthesized buried oxynitride layers in silicon*, Appl. Phys. Lett. **52**, 1871 (1988).

[48] M. Döbeli, P. Haubert, R. Livi, S. Spicklemire, D. Weathers, and T. Tombrello, *Heavy ion backscattering analysis with a time-of-flight detector*, Nucl. Instrum. Methods Phys. Res., Sect. B **47**, 148 (1990).

[49] H. J. Whitlow, H. Timmers, R. G. Elliman, T. D. Weijers, Y. Zhang, and D. O'Connor, *Measurement and uncertainties of energy loss in silicon over a wide Z1 range using time of flight detector telescopes*, Nucl. Instrum. Methods Phys. Res., Sect. B **195**, 133 (2002).

[50] H. J. Whitlow, H. Timmers, R. G. Elliman, T. D. Weijers, Y. Zhang, J. Uribastera, and D. John O'Connor, *Measurements of Si ion stopping in amorphous silicon*, Nucl. Instrum. Methods Phys. Res., Sect. B **190**, 84 (2002).

[51] Y. Zhang, G. Possnert, and H. J. Whitlow, *Measurements of the mean energy-loss of swift heavy ions in carbon with high precision*, Nucl. Instrum. Methods Phys. Res., Sect. B **183**, 34 (2001).

[52] Y. Zhang, *High-precision measurement of electronic stopping powers for heavy ions using high-resolution time-of-flight spectrometry*, Nucl. Instrum. Methods Phys. Res., Sect. B **196**, 1 (2002).

[53] Y. Zhang, W. J. Weber, and H. J. Whitlow, *Electronic stopping powers for heavy ions in silicon*, Nucl. Instrum. Methods Phys. Res., Sect. B **215**, 48 (2004).

[54] W. Trzaska, T. Alanko, V. Lyapin, and J. Räisänen, *A novel method for obtaining continuous stopping power curves*, Nucl. Instrum. Methods Phys. Res., Sect. B **183**, 203 (2001).

[55] W. Trzaska, V. Lyapin, T. Alanko, M. Mutterer, J. Räisänen, G. Tjurin, and M. Wojdyr, *New approach to energy loss measurements*, Nucl. Instrum. Methods Phys. Res., Sect. B **195**, 147 (2002).

[56] T. Alanko, W. Trzaska, V. Lyapin, J. Räisänen, G. Tiourine, and A. Virtanen, *Simultaneous wide-range stopping power determination for several ions*, Nucl. Instrum. Methods Phys. Res., Sect. B **190**, 60 (2002).

[57] B. Wilkins, M. Fluss, S. Kaufman, C. Gross, and E. Steinberg, *Pulse-height defects for heavy ions in a silicon surface-barrier detector*, Nuclear Instruments and Methods **92**, 381 (1971).

[58] E. Steinberg, S. Kaufman, B. Wilkins, C. Gross, and M. Fluss, *Pulse height response characteristics for heavy ions in silicon surface-barrier detectors*, Nuclear Instruments and Methods **99**, 309 (1972).

[59] L. Cliche, S. Gujrathi, and L. Hamel, *Pulse height defects for 16O, 35Cl and 81Br ions in silicon surface barrier detectors*, Nucl. Instrum. Methods Phys. Res., Sect. B **45**, 270 (1990).

[60] H. J. Whitlow and Y. Zhang, *Fundamental effects and non-linear Si detector response*, Nucl. Instrum. Methods Phys. Res., Sect. B **190**, 375 (2002).

[61] Y. Zhang and H. J. Whitlow, *Response of Si p-i-n diode and Au/n-Si surface barrier detector to heavy ions*, Nucl. Instrum. Methods Phys. Res., Sect. B **190**, 383 (2002).

[62] Y. Zhang, W. Weber, and C. Wang, *Electronic stopping powers in silicon carbide*, Phys. Rev. B **69**, 205201 (2004).

[63] J. Sundqvist, H. Högberg, and A. Hå rsta, *Atomic Layer Deposition of Ta2O5 Using the TaI5 and O2 Precursor Combination*, Chem. Vap. Deposition **9**, 245 (2003).

[64] K. Kukli, M. Ritala, M. Leskelä, T. Sajavaara, J. Keinonen, D. Gilmer, S. Bagchi, and L. Prabhu, *Atomic layer deposition of Al2O3, ZrO2, Ta2O5, and Nb2O5 based nanolayered dielectrics*, J. Non-Cryst. Solids **303**, 35 (2002).

[65] S. Jakobs, A. Duparré, M. Huter, and H. Pulker, *Surface roughness characterization of smooth optical films deposited by ion plating*, Thin Solid Films **351**, 141 (1999).

[66] H. Lefevre, R. Schofield, and D. Ciarlo, *Thin Si3N4 windows for energy loss STIM in air*, Nucl. Instrum. Methods Phys. Res., Sect. B **54**, 47 (1991).

[67] M. Döbeli, C. Kottler, F. Glaus, and M. Suter, *ERDA at the low energy limit*, Nucl. Instrum. Methods Phys. Res., Sect. B **241**, 428 (2005).

[68] W. Assmann, *Ionization chambers for materials analysis with heavy ion beams*, Nucl. Instrum. Methods Phys. Res., Sect. B **64**, 267 (1992).

[69] F. S. Goulding and B. G. Harvey, *Identification of Nuclear Particles*, Annual Review of Nuclear Science **25**, 167 (1975).

[70] H. Sann, H. Damjantschitsch, D. Hebbard, J. Junge, D. Pelte, B. Povh, D. Schwalm, and D. Tran Thoai, *A position-sensitive ionization chamber*, Nuclear Instruments and Methods **124**, 509 (1975).

[71] F. Naulin, M. Roy-Stephan, and E. Kashy, *Improved energy resolution in an ionization chamber through suppression of the field distortions*, Nuclear Instruments and Methods **180**, 647 (1981).

[72] W. Assmann, *Ionization chambers for materials analysis with heavy ion beams*, Nucl. Instrum. Methods Phys. Res., Sect. B **64**, 267 (1992).

[73] W. Assmann, P. Hartung, H. Huber, P. Staat, H. Steffens, and C. Steinhausen, *Setup for materials analysis with heavy ion beams at the Munich MP tandem*, Nucl. Instrum. Methods Phys. Res., Sect. B **85**, 726 (1994).

[74] W. Assmann, J. Davies, G. Dollinger, J. Forster, H. Huber, T. Reichelt, and R. Siegele, *ERDA with very heavy ion beams*, Nucl. Instrum. Methods Phys. Res., Sect. B **118**, 242 (1996).

[75] J. Forster, P. Currie, J. Davies, R. Siegele, S. Wallace, and D. Zelenitsky, *Elastic recoil detection (ERD) with extremely heavy ions*, Nucl. Instrum. Methods Phys. Res., Sect. B **113**, 308 (1996).

[76] H. Timmers, T. Ophel, and R. Elliman, *Simplifying position-sensitive gas-ionization detectors for heavy ion elastic recoil detection*, Nucl. Instrum. Methods Phys. Res., Sect. B **161-163**, 19 (2000).

[77] W. K. Chu, J. W. Mayer, and M. A. Nicolet, *Backscattering spectrometry* (Academic Press, ADDRESS, 1978).

[78] K. Schmid and H. Ryssel, *Backscattering measurements and surface roughness*, Nuclear Instruments and Methods **119**, 287 (1974).

[79] T. Sajavaara, K. Arstila, A. Laakso, and J. Keinonen, *Effects of surface roughness on results in elastic recoil detection measurements*, Nucl. Instrum. Methods Phys. Res., Sect. B **161-163**, 235 (2000).

[80] M. E. Adel, O. Amir, R. Kalish, and L. C. Feldman, *Ion-beam-induced hydrogen release from a-C:H: A bulk molecular recombination model*, J. Appl. Phys. **66**, 3248 (1989).